NTNU

Norwegian University of
Science and Technology

On the Accuracy of Mapping the Lateral Extent of Hydrocarbon Reservoirs in Marine CSEM

Karen Synnøve Ohm

Petroleum Geoscience and Engineering
Submission date: January 2016
Supervisor: Rune Mittet, IPT

Norwegian University of Science and Technology
Department of Petroleum Engineering and Applied Geophysics

Abstract

In marine CSEM it is known that the real areal extent of a hydrocarbon reservoir will not necessarily be mapped correctly during inversion. Generally, the inversion will cause the reservoir to be undersized, as a result of loss of frequencies in the subsurface. The error margin of the under sizing, and how this depends on burial depth will therefore be investigated in this study. This was done by studying the significance level of the mean squared error for a 2D model where length and burial depth of the reservoir was varied. The mean square error was found by using forward modeling where data from a set reservoir length was compared to the data for reservoirs with varied length. The data was then inverted by using Gauss Newton, where the length of the imaged reservoir was compared to the result of the forward modeling. It was found by using a statistical significance level of 10 standard deviations the change in the data fitted well with the change in the imaged model.

Sammendrag

Reservoirets utstrekning vil ikke nødvendigvis bli avbildet korrekt etter inversjon av marin CSEM data. Dette er et resultat av at høye frekvenser blir attenuert i undergrunnen. Denne oppgaven vil derav studere feilmarginen ved avbilding av et reservoir, og se hvordan feilmargingen er avhengig av begravelsesdyp. Dette blir gjort ved å studere en enkel 2D model hvor reservoirets lengde og begravelsesdyp blir variert. Minste kvadratsfeilen blir beregnet ved å sammenligne de forover modelerte dataene for en fast reservoir lengde, med de forover modelerte dataene for reservoirer med varierende lenge. Studien viser at ved å bruke en statistisk signifikanse grense på 10 standard avik, passer forandrigene i forover modelerte dataene med forandring i avbildingen av reservoiret.

Acknowledgment

I would like to thank my supervisor Rune Mittet for all the help he provided and for sharing his knowledge with me. I would also like to thank EMGS for giving me an office, letting me use their software and making me feel welcome and as a part of EMGS. And also a special thanks to Kristian Rymann Hansen for taking an interest in this study and always being available for questions. Last but not least, tanks to all my family and friends.

Contents

1 Introduction

The marine controlled-source electromagnetic (CSEM) method or seabed logging (SBL) have during the last 15 years proven successful in hydrocarbon exploration, (Ellingsrud et al., 2002; Constable, 2010; Constable and Weiss, 2006). The marine CSEM method is based on the study of the propagation of low frequency electromagnetic fields in the earth. The electromagnetic fields are useful in geophysics since they interact with the medium in which they propagate, by inducing currents that propagate through the media. From this interaction it is in principle possible to measure certain physical properties of rocks, such as the electric permittivity(ε), magnetic permeability (μ) and the electric conductivity (σ) (Norbert, 2014). The electric conductivity can provide information about the pore fluids, as well as the porosity of geological formations. The resistivity will increase with increasing hydrocarbon saturation of rocks, hence, creating a strong contrast in resistivity between hydrocarbon saturated rocks and brine saturated rocks. Marine CSEM is useful when combined with other geophysical tools such as seismic and AVO, as it helps to decrease the risk of drilling dry wells.

Even though the marine CSEM data can be useful for hydrocarbon exploration, it still has some limitations. One of the limitations is that marine CSEM can generally only detect a reservoir down to 2 to 3 km burial depth. This is a result of the skin depth effect, which causes the highest frequencies to get attenuated faster than the lower frequencies. Loss of frequencies for increasing depth will cause the resolution of marine CSEM to decreases with depth. Thus, making it difficult to accurately image a reservoir with increasing burial depth. This results in the error of the imaged reservoir to increase with burial depth, causing the imaged reservoir to be undersized.

There have been many studies regarding the sensitivity of marine CSEM in the subsurface, many of which attempts to understand how well CSEM data can actually image the subsurface. Sensitivity studies of the resistivities

in the subsurface include studies to find the best sensitivity for the survey set up. In these surveys one tries to figure out if the CSEM is able to detect the reservoir, and what is the optimal survey configuration for the marine CSEM set up (Kaputerko et al., 2007; Becken and Streich, 2010; Gao et al., 2007). Through studies of the anisotropic sensitivity in reservoirs (Streich and Becken, 2011; Brown et al., 2012), geophysicists have obtained a better understanding of the sensitivity to the reservoir and background. There have also been some studies on reservoir monitoring, and how marine CSEM is affected by a reservoir being water flooded during oil recovery (Lien and Mannseth, 2008; Orange et al., 2009; Wang et al., 2008). Along with a sensitivity study from Bhuyian et al. (2012), where the sensitivity of marine CSEM under CO_2 storage was investigated, a broader understanding of how sensitive marine CSEM is to changes in the reservoir have been reached. Other interesting sensitivity studies include Ansari et al. (2012) which studied the relationship between the resistivity contrast and the thickness, where it was found out that the higher resistivity contrast and thickness the greater the chance for for determining the reservoir by CSEM.

This study attempts to estimate the error of under sizing a reservoir and how it is linked to increasing burial depth. This was done by using a simple 2D model where the length and depth of the reservoir was varied. Forward modeling was used to get an estimate of the marine CSEM sensitivity to changes in the reservoir by studying the mean square error. This was done by studying the difference in the observed data, which represents the full size reservoir and the predicted data, which represents the undersized reservoir. To find out when the change in the data also gives a change in the image of the model after inversion, a chi squared statistical analysis is conducted to find the statistical significance level.

In the following some background about CSEM will be discussed before the theory that has been used in this master thesis is presented. Further the model and the method will be discussed, before the results of the numerical example is presented.

2 Background of Marine CSEM

In this section some background about marine CSEM will be presented, along with some theory of how marine CSEM is able to image the subsurface.

2.1 Resistivity in earth

Marine CSEM works by measuring the electromagnetic fields that propagate through the subsurface, as a result of an active source. From the electromagnetic fields it is possible to estimate the electric resistivity, ρ, in the subsurface. This can provide information about the properties of various bedrocks. The different resistivities of the common materials in the earth can be seen in Figure 1, which shows that the sedimentary rocks all shear a low resistivity, despite the fact that most of the common sedimentary rock minerals have much higher resistivities (Reynolds, 2011). The resistivity in sedimentary rocks are mainly controlled by the permeability, porosity, and the pore geometry, as well as by the pore fluids of the rocks and by temperature. Changes in the resistivity in rocks are controlled by the interaction between the high resistive minerals and pore fluids. The pore fluids can be either brine, fresh water or hydrocarbon. Seawater is a conductive medium, as seen in Figure 1, where its conductivity is dependent on the salinity of the water, the temperature and the composition of the salt. Fresh water, however, will not conduct electricity as well, since it has low salinity. Hydrocarbons have high resistivity, which can be seen in Figure 1. The resistivity will consequently increase with increasing hydrocarbon saturation (Johansen and Gabrielsen, 2015).

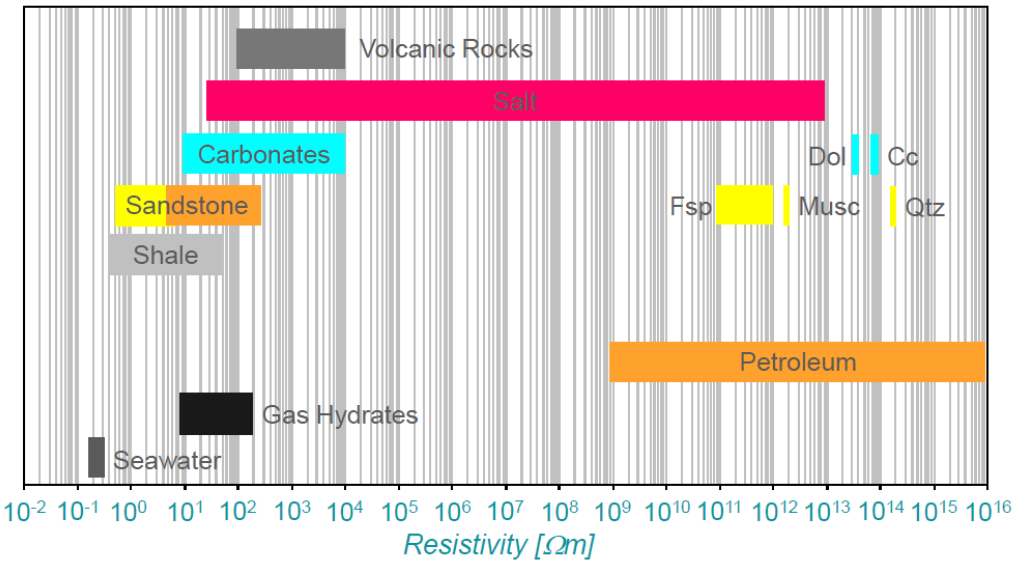

Figure 1: Typical resistivies in the subsurface, shown in a logarithmic scale. (The image is taken from EMGS internal website.)

2.2 Archie's Law

The increase in resistivity for hydrocarbon bearing rocks can be explained by Archie's law (Keller, 2006)

$$\rho_{true} = \frac{a\rho_w}{\phi^m(1 - S_H)^n}, \tag{1}$$

where ρ_{true} and ρ_w represent the formations true resistivity and resistivity of the formation water respectively. S_H is the hydrocarbon saturation, which is defined as $1 - S_w$ where S_w is the water saturation. Here, ϕ is the formation porosity. The factor a is the lithology coefficient and is set to be approximately 1. The cementation exponent, m, is a measure of how well connected the pore space is in the formation. If $m < 2$ the formation has low pore isolation, meaning that the pores are well connected. However, if $m > 2$ the formation has high pore isolation, meaning that the pores are well isolated. The saturation exponent, n, indicates whether the rock is water wet or hydrocarbon wet, and if $n > 2$ the rock has low pore isolation and is

considered to be water wet. When $n < 2$, the rock has high pore isolation which suggests that the formation is hydrocarbon wet (Archie, 1942).

Figure 2 shows how the resistivity increase with increasing hydrocarbon (HC) saturation, as a result of Archie's law. If the HC saturation is increased to more than approximately 50 % the change in resistivity will be significantly high enough to be detected by CSEM. As a comparison, the P-wave velocity is reduced quickly when only a small amount of HC saturation is introduced. However, the P-wave velocity is not sensitive to any further increase in HC saturation. The P-wave velocity is found from seismic data, which uses acoustic waves to investigate the geophysical properties in the subsurface. This means that seismic is not sensitive to the HC saturation after approximate 20 %, whereas marine CSEM only will detect a potential reservoir if the HC saturation is above 50 %. Used together marine CSEM and seismic may provide a better mapping of the subsurface.

Oil and gas will have the same effect on the electromagnetic fields, and will both increase the resistivity in a reservoir. Marine CSEM, hence, is not able to distinguish oil from gas in the subsurface.

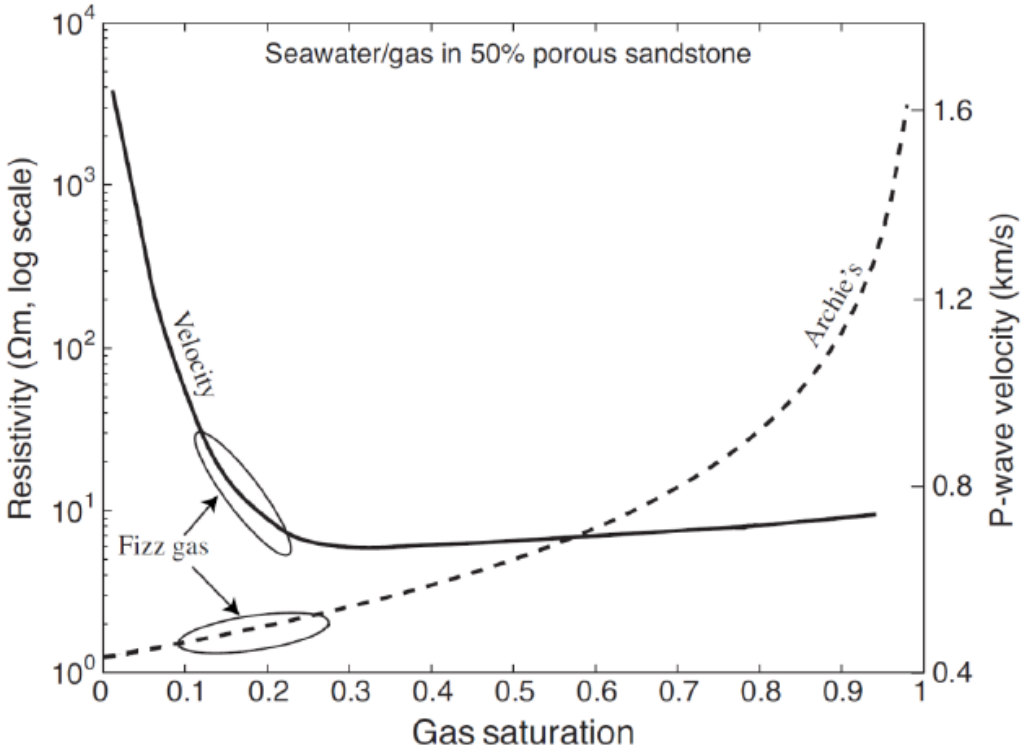

Figure 2: Resistivity and P-wave velocity as a function of hydrocarbon saturation in a 50 % porous sandstone. (Constable, 2010).

2.3 CSEM survey

Marine CSEM surveys are conducted by placing receivers at the sea bed in a grid and towing a horizontal electric dipole source over the receivers (Constable, 2010), as shown in Figure 3. The source is towed over the receivers close to the sea floor, to minimize coupling with air and to maximize coupling with the sediments. The horizontal electric dipole source emits a continued and optimized waveform signal with low frequencies, as explained by Mittet and Schaug-Pettersen (2008). When the source is towed directly over a single receiver line it is called a 2D survey. Data that are collected from this type of survey is called inline data. For a 3D survey the data are collected from a grid. Data that are collected perpendicular to the

source, are called broadside data, and data that comes from receivers placed somewhere in between inline and broadside are called azimuth data. The source and receiver configurations are shown in Figure 4. The inline data are more sensitive to the vertical resistivity component than to the horizontal resistivity component. The broadside data, however, are generally more sensitive to the horizontal resistivity component (Streich and Becken, 2011). This is illustrated in Figure 4, where the receiver in the inline configuration measure the electric field that is parallel to the propagation direction with the vertical loop. The broadside measure the electric field components that is perpendicular to the propagation direction with horizontal current loop. This is explained in more details by Constable (2010), Løseth (2007) and Chlamtac and Abramovici (1981). The receivers measure the electromagnetic fields, which are combinations of; the electromagnetic signal transmission that comes directly through the seawater, the refraction and reflection signal from the seawater-air interaction, the seawater and seabed interaction, and possibly the interaction with a thin high resistive layer. For thin high resistive layers the receivers measure the transverse resistivity, which is defined as

$$T = \Delta\rho\Delta z, \tag{2}$$

where $\Delta\rho$ is the difference in resistivity between the reservoir and the background, and Δz is the thickness of the reservoir (Mittet and Morten, 2013; Johansen and Gabrielsen, 2015).

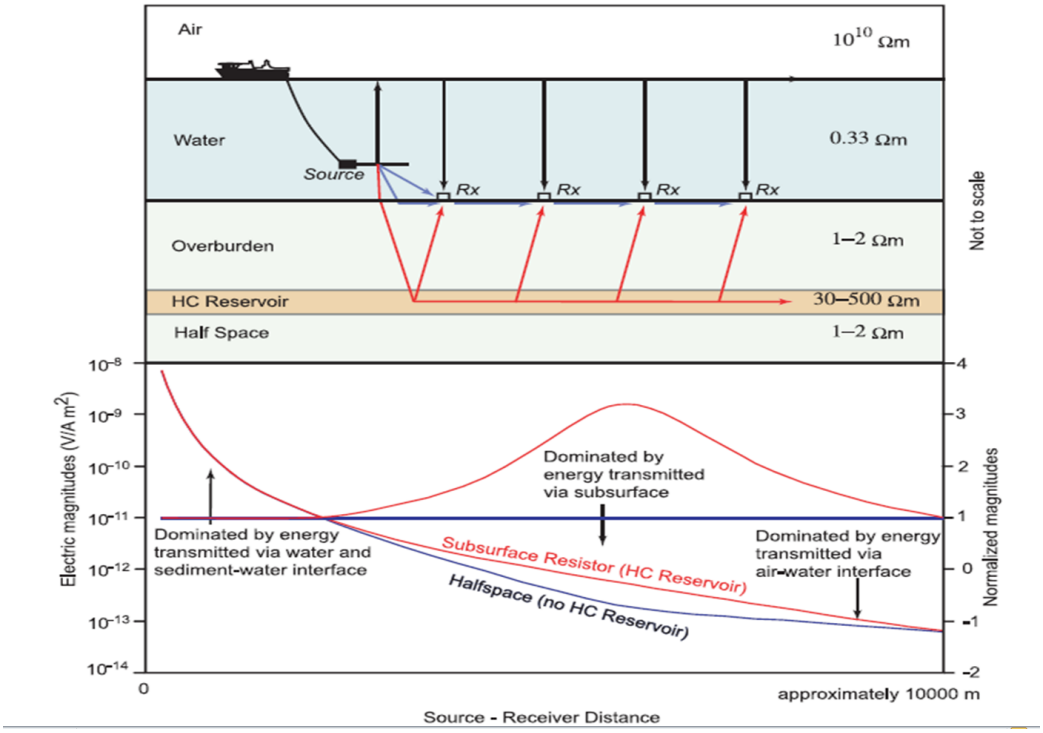

Figure 3: Upper part: Receiver and source configuration for a 2D marine CSEM survey. The horizontal dipole source is being towed over the receivers that are placed on the seabed. The receivers measure the electromagnetic fields integration with the air-water interface and the water-seabed interface, and the reflection and refraction between the overburden-reservoir layers. The air and the reservoir are resistive layers, while the sea water and seafloor has low resistivity. **Lower part**: The magnitude and phase plot of the electromagnetic field as a function of source-receiver distance. (Cox et al., 1986)

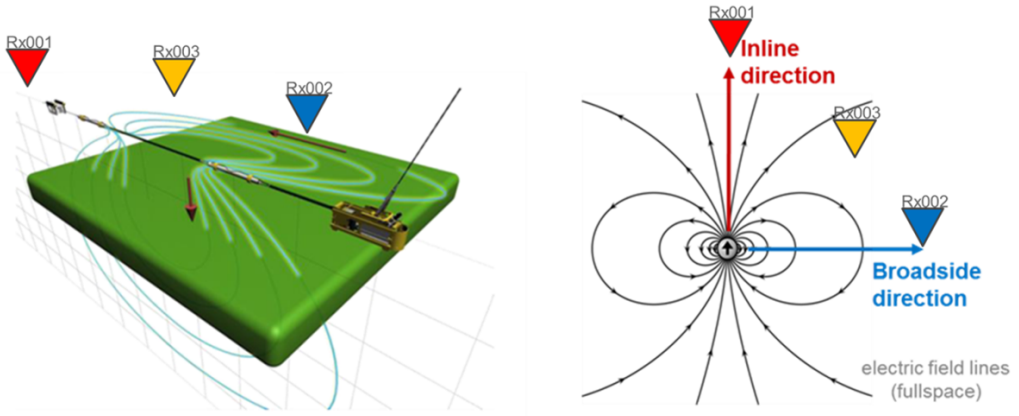

Figure 4: Source and receiver configurations. Receiver Rx001 shows the inline configuration, which measure the electric field component that are parallel to the propagation direction with vertical current loops. Receiver Rx002 show the broadside configuration, which measure the electric field components that are perpendicular to the propagation direction with a horizontal current loop. Receiver Rx003 is the azimuth configuration and will measure both the inline and broadside data. (Johansen and Gabrielsen, 2015)

2.4 Anisotropy

A medium is said to be anisotropic, when certain physical properties are directionally dependedt. The anisotropy in the earth is normally a combination of intrinsic anisotropy, which are changes within a formation like changes in grain size, shape and orientation. The other type of anisotropy is structural anisotropy, which can come from thin bedding (Keller, 2006). Ohm's law is an important relationship that explains the dependency of the electromagnetic fields and the media in which the field propagates,

$$\mathbf{J} = \sigma \mathbf{E}, \tag{3}$$

where **J** is the current density and **E** is the electric field. The conductivity, σ is a tensor

$$\sigma = \begin{bmatrix} \sigma_{xx} & \sigma_{xy} & \sigma_{xz} \\ \sigma_{yx} & \sigma_{yy} & \sigma_{yz} \\ \sigma_{zx} & \sigma_{zy} & \sigma_{zz} \end{bmatrix} \tag{4}$$

In this study the model is assumed to be transverse isotropic with a vertical axis of symmetry (TIV), which means that the electrical properties are described by a horizontal and a vertical component. This means that the off diagonal conductivities will be zero, and the x- and y- components are equal and denoted $\sigma_{xx} = \sigma_{yy} = \sigma_h$. The z- component is denoted as the vertical conductivity, $\sigma_{zz} = \sigma_v$

$$\sigma = \begin{bmatrix} \sigma_h & 0 & 0 \\ 0 & \sigma_h & 0 \\ 0 & 0 & \sigma_v \end{bmatrix} \tag{5}$$

The electromagnetic anisotropy is defined as the vertical resistivity component divided by the the horizontal resistivity component. In general the vertical resistivity component will be higher than the horizontal resistivity component due to layering in the subsurface. It is important to include anisotropy when imaging the subsurface, as one may get false inversion and interpretation results if it is excluded (Lu and Xia, 2007).

3 Theory

In order to better understand the imaging error with regards to the lateral extent and how it is dependent on the burial depth, a short summary of the CSEM theory will be presented. More specifically, the theory of how the observed and predicted data is generated will be presented, along with theory of the error estimate of the under sizing and the inversion used for calibration. The observed data represent the full size reservoir and the predicted data represent the undersized reservoir.

3.1 Maxwell's Equations

3.1.1 Maxwell's equations

Maxwell's equations describe the propagation of electromagnetic fields in any given medium. The general form of the macroscopic Maxwell's equations is

$$-\nabla \times \mathbf{H} + \frac{\partial}{\partial_t}\mathbf{D} = -\mathbf{J}, \tag{6}$$

$$\nabla \times \mathbf{E} + \frac{\partial}{\partial_t}\mathbf{B} = 0, \tag{7}$$

$$\nabla \cdot \mathbf{D} = q, \tag{8}$$

$$\nabla \cdot \mathbf{B} = 0. \tag{9}$$

Here $\mathbf{E}$ and $\mathbf{H}$ are the electric and magnetic field, and $\mathbf{B}$ is the magnetic induction while $\mathbf{D}$ is the electric displacement. The charge density is denoted as q. The current density is denoted by $\mathbf{J}$, and is defined as

$$\mathbf{J} = \sigma\mathbf{E} + \mathbf{J}^s, \tag{10}$$

where $\sigma\mathbf{E}$ is the conduction current and $\mathbf{J}^s$ is the contribution from the source current. Assuming linear and isotropic media, we get the relations $\mathbf{D} = \varepsilon\mathbf{E}$ and $\mathbf{B} = \mu\mathbf{H}$. Here ε is the electric permittivity and μ is magnetic

permeability of the medium. The magnetic permeability is defined as $\varepsilon = \varepsilon_R \varepsilon_0$, where ε_0 is the permeability in free space and ε_R is the relative permeability ratio of a certain medium. Since it is assumed that sedimentary rocks are not magnetic the relative permeability is equal to 1.

3.1.2 Maxwell's equation for CSEM

Marine CSEM is described by Maxwell's equations using the relations for a linear media. By Fourier transforming equations 6, 7 and 10 the electric current density can be described in the frequency domain

$$\mathbf{J} = (i\varepsilon\omega - \sigma)\mathbf{E} + \mathbf{J}^s. \tag{11}$$

The conductivity is much larger than the electric permittivity times frequency, $\sigma \gg \omega\varepsilon$, therefor the displacement current has a negligible contribution to the electromagnetic field. This is called the quasi-static approximation, and in the frequency domain Faraday's and Ampere's law become

$$-\nabla \times \mathbf{H} + \sigma\mathbf{E} = -\mathbf{J}^s, \tag{12}$$

$$\nabla \times \mathbf{E} - i\omega\mu_0\mathbf{H} = 0. \tag{13}$$

3.2 Skin Depth

The electromagnetic fields will be attenuated and propagate at different velocities in the subsurface. This dispersion and absorption can better be explained by reducing the electric field equations to 1D. It is hence, assumed that the earth and source is invariant in x- and y-direction, and that the source has no vertical current. Then the electric and magnetic fields become invariant in x- and y-direction. By assuming the polarization is in x-direction equations 12 and 13 can be rewritten as follows

$$\partial_z H_y + \sigma E_x = -J_x^s, \tag{14}$$

and

$$\partial_z E_x - i\omega\mu_o H_y = 0. \tag{15}$$

Analysing the electromagnetic field away from the source, equation 14 and 15 can be rewritten as

$$\partial_z^2 E_x + k_\omega^2 E_x = 0, \tag{16}$$

where the wavenumber is

$$k_\omega = \sqrt{i\omega\sigma\mu_0}. \tag{17}$$

By using the relationship,

$$\sqrt{i} = \frac{1+i}{\sqrt{2}}, \tag{18}$$

the wavenumber can be expressed as a function of the phase velocity $c(\omega)$ and the skin depth $\delta(\omega)$,

$$k_\omega = \frac{\omega}{c(\omega)} + \frac{i}{\delta(\omega)}. \tag{19}$$

The phase velocity and the skin depth are defined as,

$$c(\omega) = \sqrt{\frac{2\rho\omega}{\mu_0}}, \tag{20}$$

and

$$\delta(\omega) = \sqrt{\frac{2\rho}{\mu_0\omega}}, \tag{21}$$

respectively, where the phase velocity and skin depth both are dependent on frequency and resistivity. The phase velocity will then increase if either or both the frequency and resistivity is increased. This is typical for a dispersive system, and is a consequence of strong conductive currents. The magnetic permeability in vacuum is defined as $\mu_0 = 4\pi \times 10^{-7}\frac{H}{m}$, and inserting this value into equation 21 gives the skin depth,

$$\delta(f) = \sqrt{\frac{\rho}{\pi\mu_0 f}} \approx 500\sqrt{\frac{\rho}{f}}, \tag{22}$$

The skin depth is defined as the distance over which a plane wave is attenuated by a factor of e^{-1}. Equation 22 shows that the skin depth becomes larger for higher resistivities, which means that the attenuation is higher for lower resistivities. From equation 22 we can also see that the skin depth becomes smaller for higher frequencies, causing the higher frequencies to propagate shorter distance before getting attenuated. Lower frequencies, however, will penetrate deeper before being attenuated due to the higher skin depth (Keller, 2006).

3.3 Forward Modeling

Forward modeling is a way of determining the signal a given receiver would measure in a formation or environment by applying a set of theoretical equations for the receiver response. In this case the receiver measures the electric and magnetic fields at the seabed. The known factors that are used in order to determine the measured signal, are the transmitted signal, the earths properties and the Maxwell's equations that are relevant for this case. In this case the finite-difference time-domain method was used to estimate the receiver response (Maaø, 2007; Mittet, 2010). The Maxwell's equations can then be solved by using the finite difference method on equation 12 and 13.

To save calculation time, Fourier transform is used where the Fourier transform and its inverse, with respect to the $y-$ axis is defined as

$$\tilde{u} = \int_{-\infty}^{\infty} u(x, y, z) e^{-ik_y y} dy, \qquad u = \frac{1}{2\pi} \int_{-\infty}^{\infty} \tilde{u}(x, k_y, z) e^{ik_y y} dk_y. \tag{23}$$

In this study the model used is a 2D model with an electromagnetic field propagating i 3D. By applying the Fourier transform to equations 12 and 13 a set of 2D equations are solved for 15-20 wavenumbers. By summing over the wavenumbers the electromagnetic field will propagate with a 3D geometrical spreading. The modeling of a 3D field propagating in a 2D model is often

referred to as a 2.5D modeling.

3.4 Noise

As explained before, the forward modeling calculates the observed and predicted data in a given model. To make the observed data more realistic they have been contaminated with noise. The predicted data, however, do not have any noise added to them. The observed data can be defined as

$$E_x^{obs} = (1+\beta)E_x^{mod} + \gamma_E, \tag{24}$$

and

$$H_y^{obs} = (1+\beta)H_y^{mod} + \gamma_H, \tag{25}$$

where E_x^{mod} and H_y^{mod} is the modeled electric and magnetic field given the true reservoir geometries. The term β is the multiplicative uncertainty contribution and γ_E and γ_H represent the ambient noise in the electric and magnetic field respectively. Both β and γ is normally distributed and complex numbers. The ambient noise is the noise the receiver measures, that either comes from the surroundings such as magnetotelluric noise, swell noise, and/or motion noise. It may also be internal noise from receivers, electrodes and amplifiers. The uncertainty in the data have the form,

$$\delta E_x(i) = \sqrt{\alpha^2 |E_x(i)|^2 + \eta_E^2}, \tag{26}$$

and

$$\delta H_y(i) = \sqrt{\alpha^2 |H_y(i)|^2 + \eta_H^2}, \tag{27}$$

as presented by (Mittet and Morten, 2012). The i represent the data points where the data points consist of the source position $\vec{x_s}$, receiver position $\vec{x_r}$ and frequency ω. One data point is denoted as $i = \{\vec{x_s}, \vec{x_r}, \omega\}$. Here α is the standard deviation of β and have a value of 0.02, and η is the standard deviation of γ with an electric standard deviation of $\eta_E = 10^{-10}\frac{\mathrm{V}}{\mathrm{m}}$ and a magnetic standard deviation of $\eta_H = 10^{-8}\frac{\mathrm{A}}{\mathrm{m}}$.

3.5 General Inversion Theory

Inversion is the method of finding the model that best explains the observed data. In an attempt to find this model the misfit function was minimized as shown in Figure 5, where the important steps in inversion are shown. To find the model that gives an acceptable misfit an initial guess of the model was first made, and if the misfit function was not acceptable then the model was updated. There are many different ways of updating the model, but in this study the Gauss Newton method was used. After the the model is updated, the predicted data is calculated by forward modeling. The model used in this experiment is a 2D model with an electromagnetic field propagating in 3D.

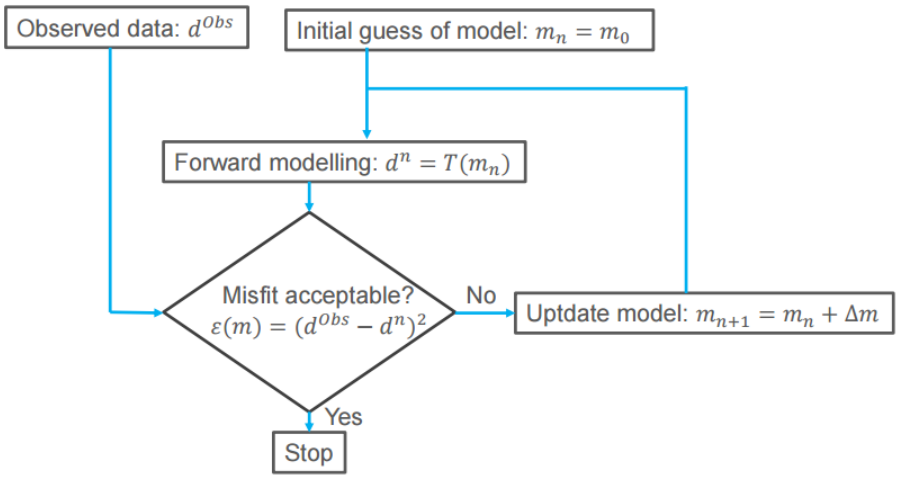

Figure 5: Setup for inversion. If the misfit between the observed (d^{Obs}) and predicted (d^n) data is not acceptable, the model will be updated and the process repeated until an acceptable misfit is reached. (Figure is taken from EMGS internal pages.)

To fit the observed data with the predicted data it is a goal to minimize the

misfit function, which is a sum over N observations.

$$\varepsilon = \sum_{i=1}^{N} \left(\frac{\left(E_x^{obs}(i) - E_x^{pred}(i)\right)^* \left(E_x^{obs}(i) - E_x^{pred}(i)\right)}{\delta E_x^2(i)} + \frac{\left(H_y^{obs}(i) - H_y^{pred}(i)\right)^* \left(H_y^{obs}(i) - H_y^{pred}(i)\right)}{\delta H_y^2(i)} \right). \tag{28}$$

Here $E_x^{obs}(i)$ and $H_y^{obs}(i)$ is the observed electric and magnetic field in the x- and y-direction respectively and $E_x^{pred}(i)$ and $H_y^{pred}(i)$ is the predicted electric and magnetic field respectively in the x- and y-direction. The complex conjugate is described by * and the term $\delta E_x(i)$ and $\delta H_x(i)$ is the data uncertainty.

3.6 Regularization

The inversion problem for electromagnetic data is ill posed, which may give the solution some undesired properties. To help stabilize the solution a regularization term, ε_R, is added to the misfit function

$$\varepsilon = \sum_{i=1}^{N} \left(\frac{\left(E_x^{obs}(i) - E_x^{pred}(i)\right)^* \left(E_x^{obs}(i) - E_x^{pred}(i)\right)}{\delta E_x^2(i)} + \frac{\left(H_y^{obs}(i) - H_y^{pred}(i)\right)^* \left(H_y^{obs}(i) - H_y^{pred}(i)\right)}{\delta H_y^2(i)} \right) + \varepsilon_R. \tag{29}$$

The regularization is defined as

$$\varepsilon_R = \int |\vec{v}|^L \, d\vec{x} d\vec{z}, \tag{30}$$

where $\vec{v}$ is defined as

$$\vec{v} = \begin{bmatrix} \alpha_x \partial_x \ln \sigma \\ \\ \alpha_z \partial_z \ln \sigma \end{bmatrix} \tag{31}$$

where σ is the conductivity and α is the expectation of how the model will look (Hansen and Mittet, 2009). In this study $\alpha_x = 1$ and $\alpha_z = 0.03$, since we have a 2D model and therefore only expect changes in the conductivity in the vertical direction. This regularization term is a smoothness factor, and will always try to find the smoothest model. We chose to use a L1 norm for the regularization, as it will image the reservoir sharply.

It is important to note that the misfit equation will be used for two purposes in this study. First, equation 28 will be solved by forward modeling to find the sensitivity to the reservoirs length, and how it depends on the burial depth. Second, equation 29 will be solved during the Gauss Newton inversion to calibrate the results from the sensitivity study. The regularization term in equation 29 is necessary when doing inversion.

3.7 Mean Square Error

The mean squared error is needed to study the sensitivity of the CSEM data. The mean square error is found by solving equation 28 to find the misfit between the observed and predicted data. For simplicity, the explanation of the mean squared error will only focus on the electric fields in this section. However, the process is exactly the same for the magnetic field. The mean squared error, $\bar{\varepsilon}^2$, is defined by

$$\bar{\varepsilon}^2 = \frac{\varepsilon}{N}. \tag{32}$$

Here, N is the number of observations. As explained above the observed data is contaminated with noise, while the predicted data are noiseless. The misfit function from equation 28 can then be written in terms of equation 24

$$\varepsilon = \sum_{i=1}^{N} \frac{(\beta E_x^{mod}(i) + \gamma - E_x^{pred}(i)) * (\beta E_x^{mod}(i) + \gamma - E_x^{pred}(i))}{\delta E_x^2(i)}. \tag{33}$$

Assuming the predicted conductivity model is equal to the true conductivity model, the predicted data is equal to the modeled data.

$$\varepsilon = \sum_{i=1}^{N} \frac{(\beta E + \gamma) * (\beta E + \gamma)}{\alpha^2 E_x^{obs2} + \eta_x^2} \rightarrow N. \tag{34}$$

By summing over a large number of observations the noise in the data will approach the same value, making equation 34 approach the number of observations.

3.8 Gauss Newton Inversion

To calibrate the results from the sensitivity study, the results from the forward modeling was inverted by using the Gauss Newton method (Nocedal and Wright, 2000). The Gauss Newton inversion is solved by minimising the misfit equation, equation 29. In this section the term from the magnetic field is neglected and it is only focused on the electric field as the procedure is the same for both fields. Also, the regularization term is neglected the derivation for the inversion. The uncertainty contribution in equation 26 can be written as a weighting function

$$W(i) = |\delta E_x(i)|^{-2}. \tag{35}$$

By placing equation 35 into equation 28 one obtains the equation

$$\varepsilon(\vec{\sigma}) = \sum_{i=1}^{N} W(i) \left(E_x^{obs}(i) - E_x^{pred}(i)(\sigma)\right)^* \left(E_x^{obs}(i) - E_x^{pred}(i)(\sigma)\right). \tag{36}$$

Here $\vec{\sigma}$ represent every pixel of the vertical (σ_v) and horizontal (σ_H) conductivity. By Taylor expanding this expression with respect to a small increase in the conductivity, one gets

$$\begin{aligned} \varepsilon(\sigma + \Delta\sigma) = \sum_{i=1}^{N} W(i) &\left(E_x^{obs}(i) - E_x^{pred}(i)(\sigma) - \frac{\partial E_x^{pred}(i)}{\partial \sigma_k}\Delta\sigma_k\right)^* \\ &\left(E_x^{obs}(i) - E_x^{pred}(i)(\sigma) - \frac{\partial E_x^{pred}(i)}{\partial \sigma_k}\Delta\sigma_k\right), \end{aligned} \tag{37}$$

where $\frac{\partial E_x}{\partial \sigma_k}$ is the Fréchet derivative which describe how the data change with respect to σ_k. Here k is the index of the vector $\vec{\sigma}$ and runs over all the pixels in the model. In order to find the minimum of the misfit function, one differentiate the misfit function with respect to the small increase in conductivity, and equals the derivative to zero,

$$\frac{\partial \varepsilon(\vec{\sigma} + \Delta\vec{\sigma})}{\partial \Delta\sigma_j} = 0, \tag{38}$$

this gives

$$\begin{aligned} 0 = \sum_{i=1}^{N} W(i) \Bigg\{ \left(-\frac{\partial E_x(i)}{\partial \sigma_j} \right)^* \left(\Delta E_x(i) - \frac{\partial E_x(i)}{\partial \sigma_k} \Delta\sigma_k \right) + \\ \left(-\frac{\partial E_x(i)}{\partial \sigma_j} \right) \left(\Delta E_x(i) - \frac{\partial E_x(i)}{\partial \sigma_k} \Delta\sigma_k \right)^* \Bigg\}. \end{aligned} \tag{39}$$

From here on it is possible to reorganize equation (39) and solve it with respect to the conductivity, which gives the normal equations

$$\begin{aligned} \sum_{i=1}^{N} W(i) \left\{ \frac{\partial E_x(i)}{\partial \sigma_j}^* \frac{\partial E_x(i)}{\partial \sigma_k} \Delta\sigma_k + \frac{\partial E_x(i)}{\partial \sigma_j} \left(\frac{\partial E_x(i)}{\partial \sigma_k} \Delta\sigma_k \right)^* \right\} = \\ \sum_{i=1}^{N} W(i) \left\{ \left(\frac{\partial E_x(i)}{\partial \sigma_j} \right)^* \Delta E_x(i) + \left(\frac{\partial E_x(i)}{\partial \sigma_j} \right) \Delta E_x(i)^* \right\}. \end{aligned} \tag{40}$$

After summing over all the observations, equation 40 can be written as a system of linear equations

$$H^D_{kj} \Delta\sigma_j = -g^D_k, \tag{41}$$

where g^D_k is the data space gradient and H^D_{kj} is a (N×N) matrix. Let H_{kj} be the approximate Hessian matrix defined as $H_{kj} = H^D_{kj} + H^R_{kj}$, where H^D_{kj} and H^R_{kj} is the Hessian to the data and the regularization respectively. The approximate Hessian matrix to the data (H^D_{kj}) is positive semi definite, which means that the approximate Hessian matrix for the regularization (H^R_{kj}) must be defined in such a way that the approximate Hessian (H_{kj}) is positive definite. This approximate Hessian must be positive definite for the normal

equations to be solved. The solution then formally becomes

$$\Delta\sigma_j = -H_{kj}^{-1} g_k, \tag{42}$$

where g_k is defined as $g_k = g_k^D + g_k^R$, where g_k^R is the contribution of the regularization.

3.9 χ^2 Statistical Distribution

The residuals in equation 28 are closely related with the χ^2 probability density function (Walpole et al., 2007a). The χ^2 test has therefore been used to see whether a perturbation in the model parameters will give a significant change in the data. The derivation of the statistical significance level is only explained for the electric field, however, both the electric and magnetic field is included in the result. The function Q, is define as Q = 2Nε. where ε is the misfit function from equation 28. The function Q is therefore

$$Q = 2\sum_{i=1}^{N} |r_i|^2, \tag{43}$$

where the residuals are

$$r_i = \frac{E_x^{obs}(i) - E_x^{pred}(i)}{\delta E_x^{obs}(i)}. \tag{44}$$

The null hypothesis is taken to be:
$\mathbf{H}_0$: The residuals are Gaussian distributed, with variance equal to 1 and zero mean
and the alternative hypothesis is
$\mathbf{H}_1$: The residuals are Gaussian distributed, with variance equal to 1 and the mean is not equal zero.

If it is assume that the null hypothesis is true, then the Q have a chi squared distribution with $2N$ degrees of freedom due to the fact that the residuals are complex numbers with independent real and imaginary parts. The mean for the distribution is $\mu_Q = 2N$ and the variance is $\kappa_Q^2 = 4N$ (Walpole et al., 2007b). When N approaches a large number ($N \to \infty$), the distribution Q will approach the normal distribution (Walpole et al., 2007c). By rewriting the misfit function as follows

$$\varepsilon = \frac{Q}{2N} = \frac{1}{N}\sum_{i=1}^{N}\frac{|E_x^{obs}(i) - E_x^{pred}(i)|^2}{|\delta E_x^{obs}(i)|^2}, \tag{45}$$

the mean and variance of the misfit function can be found. The mean $\mu_\varepsilon = 1$ and the variance is then $\kappa_\varepsilon^2 = \frac{1}{4N^2}\kappa_Q^2 = \frac{1}{N}$. This gives a standard deviation of $\kappa_\varepsilon = \frac{1}{\sqrt{N}}$.

Even though the null hypothesis is true and the observed and predicted data are indistinguishable or not statistical significant different, one can not conclude that the models are identical. If the alternative hypothesis is true and the residuals are not zero mean, then the predicted and observed data are not equal. It can therefor be assume that the model from the predicted data is not the same as the model from the observed data.

We set the significance level so that the probability is large for a random sample to fall within a given interval (Walpole et al., 2007d). By assuming that the null hypothesis is true, the probability of measuring a misfit value that differs from 1 by Kκ is so low that the null hypothesis is rejected, where K is a positive integer. At the outset we assume K=5.

Even though the difference in data may be statistically significant, the data may not give a significance change in the image of the model after inversion. Thereby it is important to adjust the significance level to represent a significant change in imaging the reservoir.

4 Sensitivity Analysis of the Resolution to a Reservoir

In order to find an estimate of the error which causes the length of a reservoir to be undersized during inversion, a numerical experiment was conducted. In this section the method and result from the numerical experiment is discussed.

4.1 Model

In order to study the sensitivity of CSEM data to the length of a reservoir and how this depends on burial depth, a 2D model was used. The model is 8 km deep and has a length of 50 km with origo placed in the middle, as seen in Figure 6. The model consist of a sea water layer and a halfspace with a reservoir placed in the upper part of the halfspace. As seen in Figure 6 this model is a deep water case with the seabed at 2000 m depth. At the seabed 29 receivers have been placed with a spacing of 1 km. The sea water has a resistivity of 0.3125 Ωm, and the halfspace has a resistivity of 2.0 Ωm. The model is anisotropic with the anisotropic ratio set to be 2. The reservoir is placed in the middle of the model at a depth of 1000 m below the seabed. The burial depth of the reservoir will, however, be varied as part of this analysis. The length of the reservoir is 6 km, so that it extend 3 km away from the origin in both directions, and the reservoir has a thickness of 100 m. The reservoir length will also be varied as part of this analysis. The reservoir has a vertical resistivity of 50 Ωm, making the transverse resistance 5000 Ωm. A horizontal electric dipole source is assumed to be 500 m and is towed over the receivers emitting a current of 2000 A with four frequencies; 0.25, 0.50, 1.00 and 2.00 Hz. The towing of the source is started 10 km before the first receiver, and is towed to 10 km after the last receiver. This is done since a potential reservoir is only detectable for large offsets. The receivers measure the electric and magnetic field in $x-$, and $y-$direction respectively.

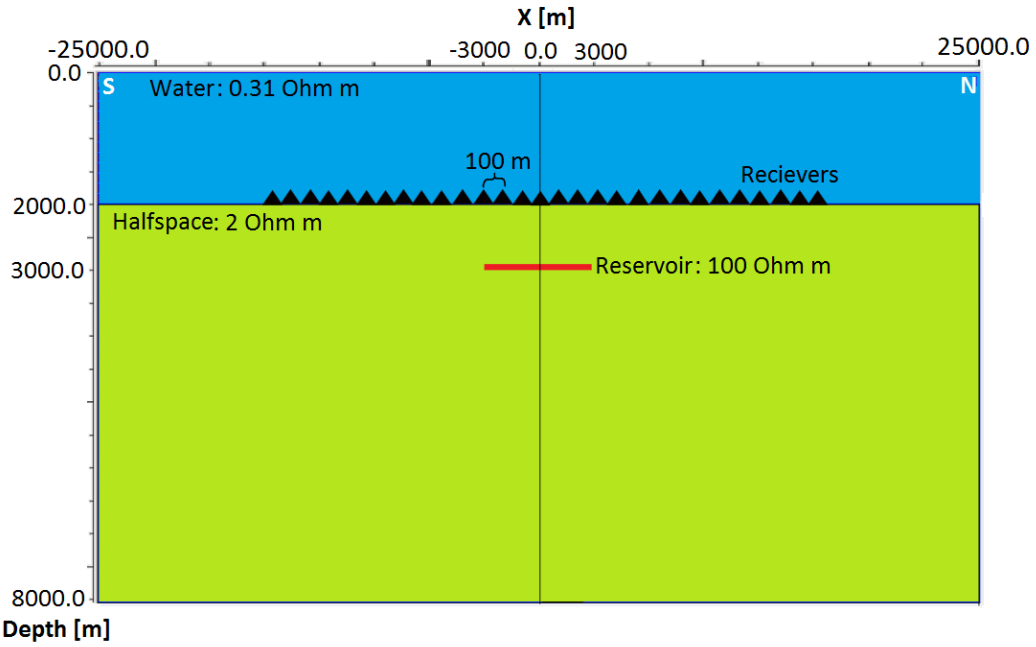

Figure 6: The figure shows the water layer with a resistivity of 0.31 Ωm, and the halfspace with a resistivity of 2 Ωm. The modeled reservoir has a length of 6 km, a thickness of 100 m and a resistivity of 100 Ωm.

4.2 Mean Squared Error

To test how well marine CSEM monitor the lateral extent of a reservoir and how it depends on burial depth, the model explained in the previous chapter was used. The sensitivity was investigated by studying the case when the reservoir's length was gradually reduced from maximum 7 km to minimum 3.7 km. The reservoir was reduced equally in both ends, with a total stepwise reduction of 100 m. For each step, forward modeling was run to find the expected response from the receivers for each depth interval. Forward modeling was used to study the sensitivity because it uses less computer time then inversion and hence, makes it possible to test several different scenarios. For a given depth the forward modeling produce observed data for the model where the reservoir's length is 6 km. Forward modeling will

also produce predicted data, which is determined from the case where the reservoir's length is gradually reduced by 100 m. The misfit between the observed and predicted data, described by equation 28, is then used to find the mean squared error by using equation 32, which indicates the sensitivity to the reservoir's length. This process is then repeated for several burial depths by increasing it successively from 1000 m to 4000 m. The burial depth was increased by 100 m in each step. For the case where the reservoir has a length of 6 km in the observed data, the model for the predicted and observed data will be the same. This will then give a mean squared value of about 1, as the noise in the data will approach the same value as the uncertainty estimate, after summing over a large number of observations.

To find the data from the resolution analysis that was statistically significant, the χ^2-distribution from section 3.9 was used. With the initial assumption that the data needs to differ more than 5κ from 1 to be statistical significant, the significance level can be calculated. The assumption of 5κ as the significance level will be calibrated later in the study. The assumption is equal to $5\frac{1}{\sqrt{\mathrm{N}}}$, where N is the number of observations. In this model we have 201 source points, 4 frequencies, 29 receivers and the field components which consists of the electric and magnetic field. Given this, the number of observations are 46632, and the assumption is then calculated to be 0.02315. The significance level is then defined as $1 \pm 5\frac{1}{\sqrt{\mathrm{N}}} = (1.02315, 0.9768)$, and all mean squared errors above 1.02315 or below 0.9768 would be considered significant.

The total mean squared error for each case has been plotted in Figure 7. In this figure only the mean squared results from forward modelling of the burial depths 1000 m to 3000 m, and the reduction of reservoir length from 7000 m to 5000 m by forward modeling are shown. Figure 7 shows how total mean squared error versus reservoir length varies with burial depth. Figure 7a focuses on the depth interval 1000 m to 2000 m and Figure 7b on the depth interval 2100 m to 3000 m. Figure 7 shows that the mean squared error fluctuates around 1, when the reservoir length for both the predicted and observed data is 6000 m. This is caused by the noise in the observed

data, and since the noise is random it will vary to some degree. Another clear trend in Figure 7 is that the total mean squared error decreases the deeper the reservoir is buried. This suggests that the sensitivity of marine CSEM decreases with increasing burial of the reservoir.

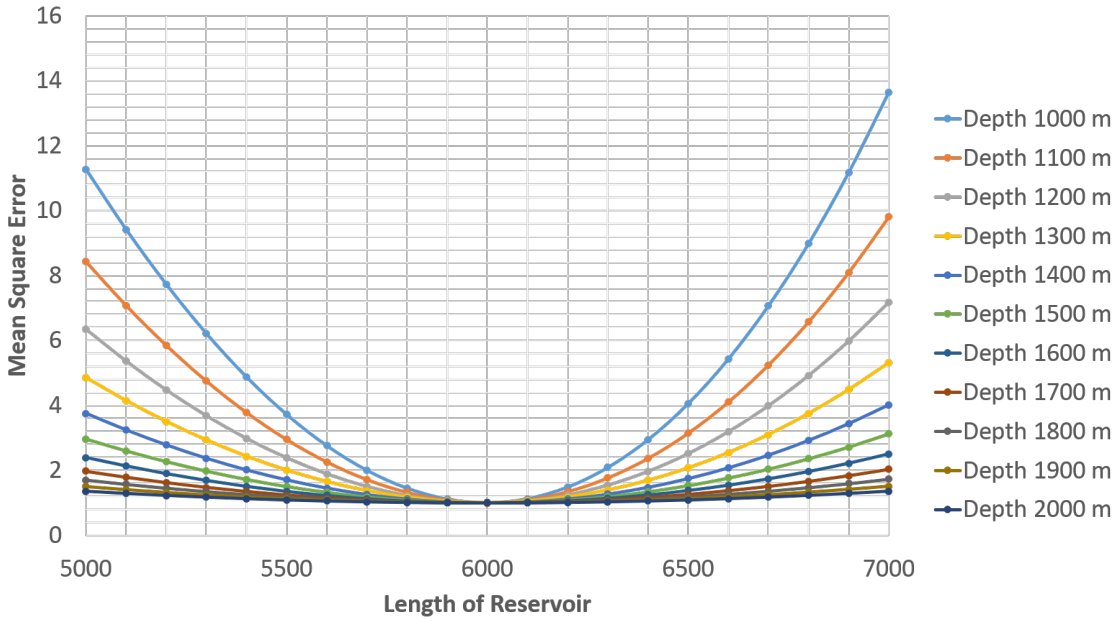

(a) Depth from 1000 m to 2000 m.

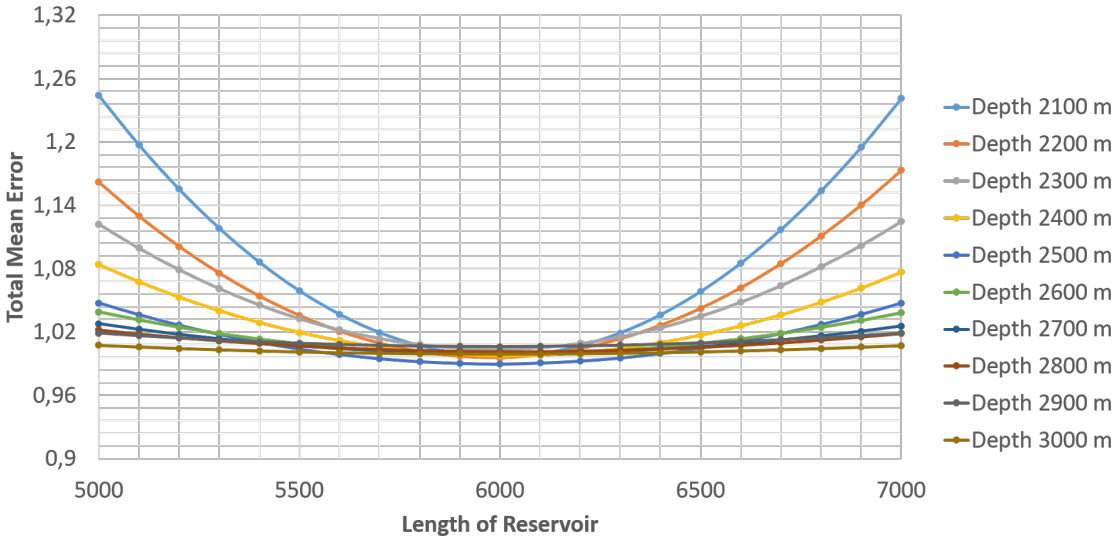

(b) Depths from 2100 m to 3000 m.

Figure 7: The total mean squared error for when the reservoir has been reduced in both ends, with a total reduction of 100 m.

Reservoirs tend to get undersized when imaged by inversion, it will hence forth only be focused on the reduction of the reservoir from 6000 m.

All the mean squared values above 1.02315, from Figure 7, are considered to be statistical significant, and Figure 8 shows the minimum perturbation size that the reservoir can have to be statistically significant related to burial depth. It is seen that the perturbations needed to get a significant result increases with burial depth.

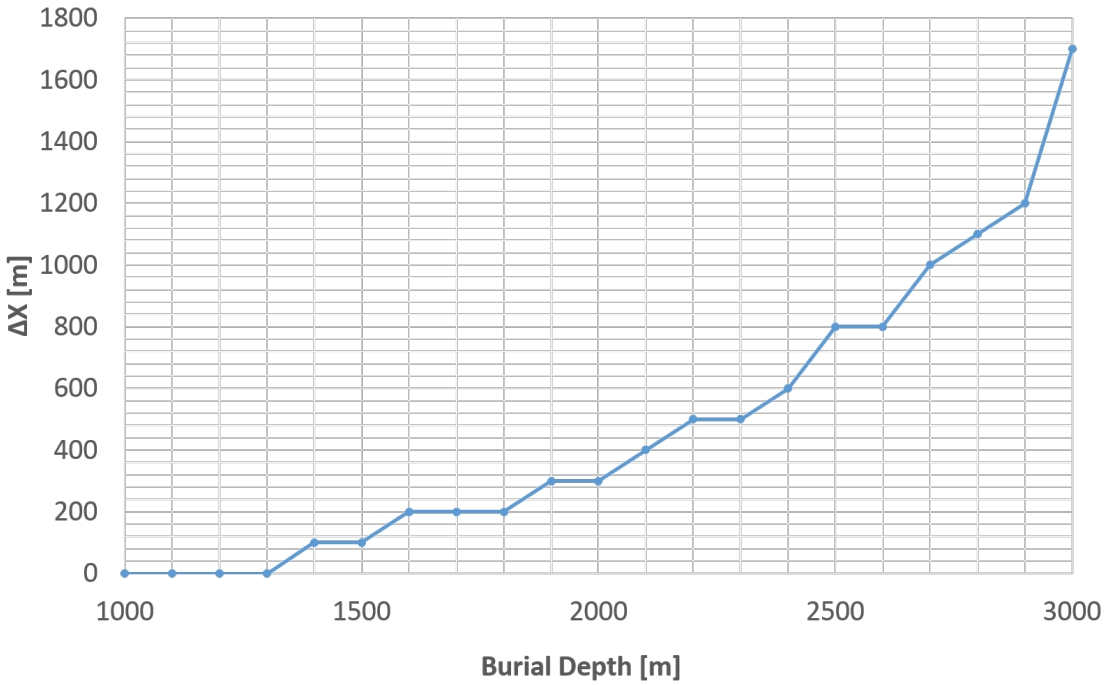

Figure 8: The reservoirs perturbation from its true length at different burial depths. Here, Δx is the change the reservoir has from it's true size of 6 km.

4.3 Loss of Frequencies

Figures 9 to 12 show the mean squared error per receiver for the four frequencies used in this model, 0.25, 0.50, 1.00 and 2.00 Hz, and how they vary for each receiver at different burial depths. Using the theory of the χ^2-distribution, which is described in section 3.9, it is possible to find when the data from Figures 9 to 12 is significant. It is initially assumed that the statistical significance level is at 5κ, where $5\kappa = \frac{5}{\sqrt{N}}$ and N is the number of observations.

However, this assumption will be calibrated later in this study, and may therefore not be correct. For this case the number of observations is a sum of all the 201 source points and fields components which include the electric and magnetic field. Given this the $5\kappa = 0.2493$, and all values above the $1 + 5\kappa = 1.2493$ significance level is considered to be significant. Even though the number of observations are only 402, the χ^2 distribution will still approach a normal distribution making the assumption of the significance value is valid. These figures are taken for the model where the reservoir has a length of 5300 m.

In Figure 9 the reservoir is buried to 1000m, and it is seen that receiver number 4 to 26 is sensitive to the perturbation in the reservoir. From the figure it is clear that all the frequencies have values above the significance level of 1.2493, and are therefore sensitive to the change in the reservoir's length. However, the frequency of 0.50 Hz seem to be most sensitive to the change, whereas the frequency of 2.00 Hz is the least sensitive of the four frequencies. Comparing Figure 9 to Figure 7 when the reservoir has a length of 5300 m and a burial depth of 1000 m, one can see that the figures matches each other well, as the mean squared error is 6.21 which is way above the significance level.

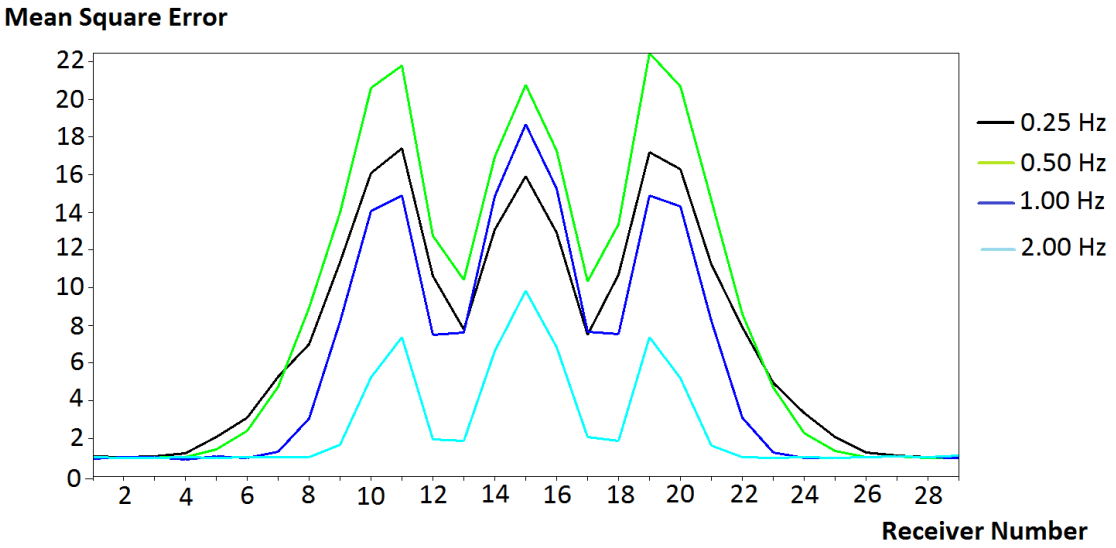

Figure 9: The mean squared error for the frequencies 0.25, 0.50, 1.00 and 2.00 Hz, as a function of receivers. The reservoir is buried to a depth of 1000 m, and has a length of 5300 m. All the frequencies are above the significance level of 1.02315

In Figure 10 the reservoir is buried to a depth of 2000 m, and the receivers are sensitive to the perturbation in the reservoir's length from receiver number 4 to 26. Figure 10 shows that only the two lowest frequencies have mean squared values that are significantly higher than 1.2493, thus, making them sensitive to the change in the reservoir's length. The two highest frequencies fluctuates around the value 1, making it unlikely that they are able to detect the change in the reservoir's length. It is, however, clear that the sensitivity for the higher frequencies is lower than for the lower frequencies. It is seen from equation 22 that higher frequencies get faster attenuated in the subsurface as a result of the skin depth effect than lower frequencies. The frequencies in Figure 10 all have lower mean squared errors than the frequencies in Figure 9 where the reservoir is buried 1000 m shallower. This loss of sensitivity is also a result of the skin depth effect, causing the field to get attenuated as they propagate through the medium. Compared to Figure 7, the mean squared value for a reservoir length of 5300 m at a burial depth of 2000 m, is 1.17. This result fit well with the mean squared result per

frequency, as they both are above the significance level and manage to detect the change in reservoir, although the resolution has decreased.

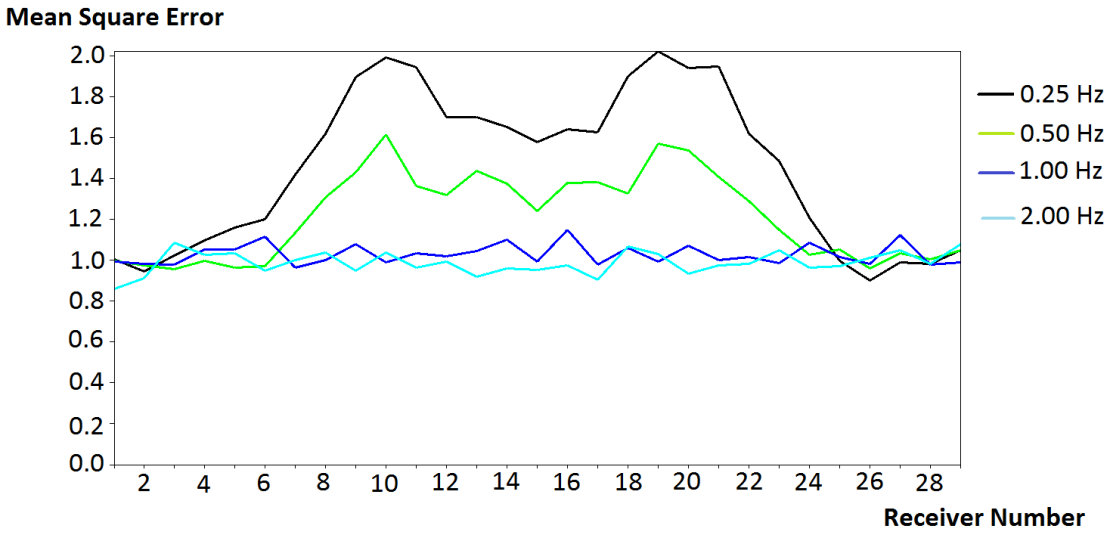

Figure 10: The mean squared error for the frequencies 0.25, 0.50, 1.00 and 2.00 Hz, as a function of receivers. The reservoir is buried to a depth of 2000 m, and has a length of 5300 m. The two lowest frequencies are above the significance level of 1.02315.

The reservoir is buried to a depth of 2500 m in Figure 11, and the receivers seem to be able to detect the perturbation in the reservoir from receiver number 5 to 25 for frequency 0.25 Hz. From Figure 11 it seems that the lowest frequency of 0.25 Hz has the highest sensitivity to the changing reservoir length, with a mean squared value of about 1.2 at its peak. The mean squared error for the lowest frequency is barely above the other frequencies, which all fluctuate around 1. The low mean squared error for the frequencies is a result of the reservoir being buried so deep that most of the frequencies have been attenuated due to the skin depth effect. Figure 11 matches Figure 7, since the total mean squared error for a reservoir length of 5300 m at 2500 m burial depth is 1.01, which is below the significance level. Even though the frequency of 0.25 Hz has values above the significance level, the total mean squared error is below, and will not reach the 5κ until the reservoir has a

length of 5000 m, as seen in Figure 8.

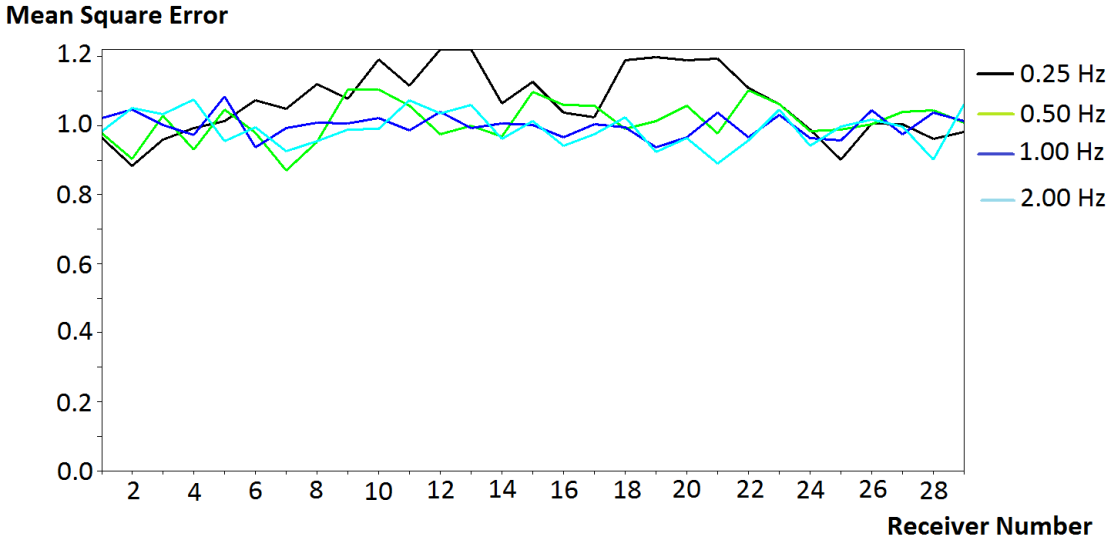

Figure 11: The mean squared error for the frequencies 0.25, 0.50, 1.00 and 2.00 Hz, as a function of receivers. The reservoir is buried to a depth of 2500 m, and has a length of 5300 m. Only the lowest frequency is above the significance level of 1.02315.

In Figure 12 the reservoir is buried to a depth of 3000 m below seabed. In this figure one can observe that all the four frequencies seem to fluctuate around the mean squared error of 1. This suggests that at this burial depth all the frequencies have been attenuated before reaching the receivers due to the skin depth effect. When comparing this result to Figure 7 and 8 a good fit is seen, as the total mean squared error for a reservoir length of 5300 m at a burial depth of 3000 m, is 1,001, and the result is therefor not significant.

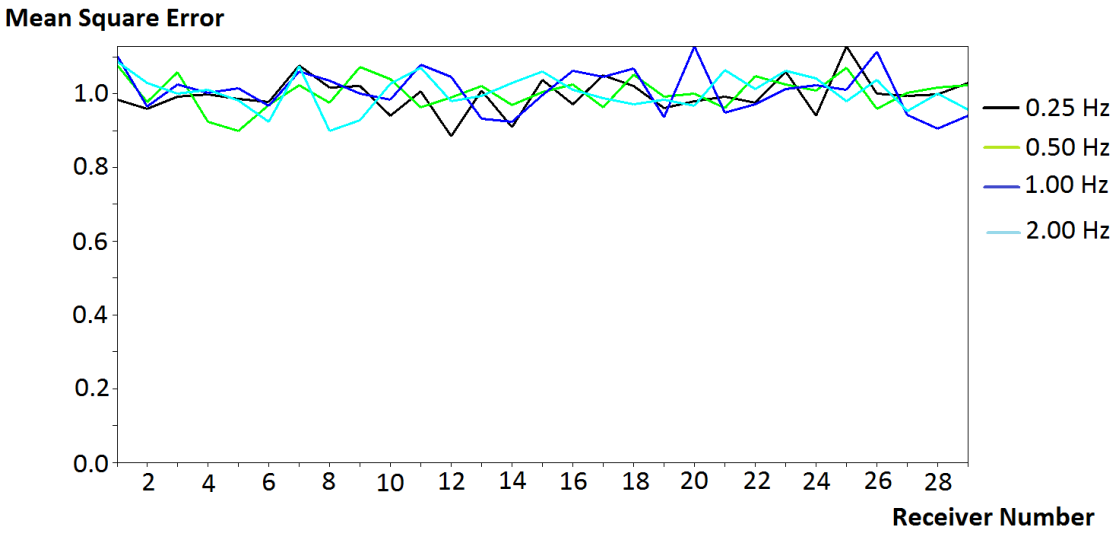

Figure 12: The mean squared error for the frequencies 0.25, 0.50, 1.00 and 2.00 Hz, as a function of receivers. The reservoir is buried to a depth of 3000 m, and has a length of 5300 m. None of the frequencies are above the significance level of 1.02315

The Figures 9 to 12 are good examples of how the frequencies will be attenuated in the subsurface. The higher frequencies can not propagate deep into the subsurface and back up to the receivers, as they will get attenuated quickly. The frequencies in the lower end of the scale can however, propagate further down into the subsurface before they are attenuated. It is still important to use a specter of frequencies when doing a marine CSEM survey, as the higher frequencies have a better resolution despite being attenuated faster.

4.4 Calibrating the Results

4.4.1 Inversion Results

The sensitivity analysis, described in Figure 7, where the total mean squared error was investigated for different reservoir lengths and burial depths, needed to be calibrated to make sure that the mean squared results fitted with how

the model would be imaged by marine CSEM inversion. The Gauss Newton inversion was used to image the model. It was decided to only run inversion over five burial depths for the calibration. The five burial depths were: 1000 m, 2000 m, 2500 m, 3000 m and 4000 m. This was done in order to calibrate the mean squared results for the different cases where the frequencies have been attenuated for increasing burial depths. It is also important to find the limit where the marine CSEM is not able to detect the reservoir. The inversion results can be viewed in Figures 13 to 17. In Figures 13 to 16 it can be seen that the imaged reservoir is not mapped with sharp edges, and that the deeper the reservoir is buried the softer the edges become. This makes it somewhat difficult to measure the true length of the reservoir, but it was decided to measure the imaged reservoirs length at the first significant increase in resistivity.

Figure 13 shows the inversion result for the case when the reservoir is buried to 1000 m. The reservoir is clearly mapped in Figure 13, and has a resistivity of about 50 Ωm. The imaged reservoir length is measured to be 6 km, from where the first significant increase in resistivity occurs. The thickness is measured to be 100 m, and the imaged reservoir is measured to have been pulled up a 100 m from the original burial depth of 1000 m. The transverse resistance of the mapped reservoir is measured to be approximately 4300 Ωm, which is a decrease from the transverse resistance in the model of 5000 Ωm. The total misfit of the inversion is 1.042 after 98 iterations.

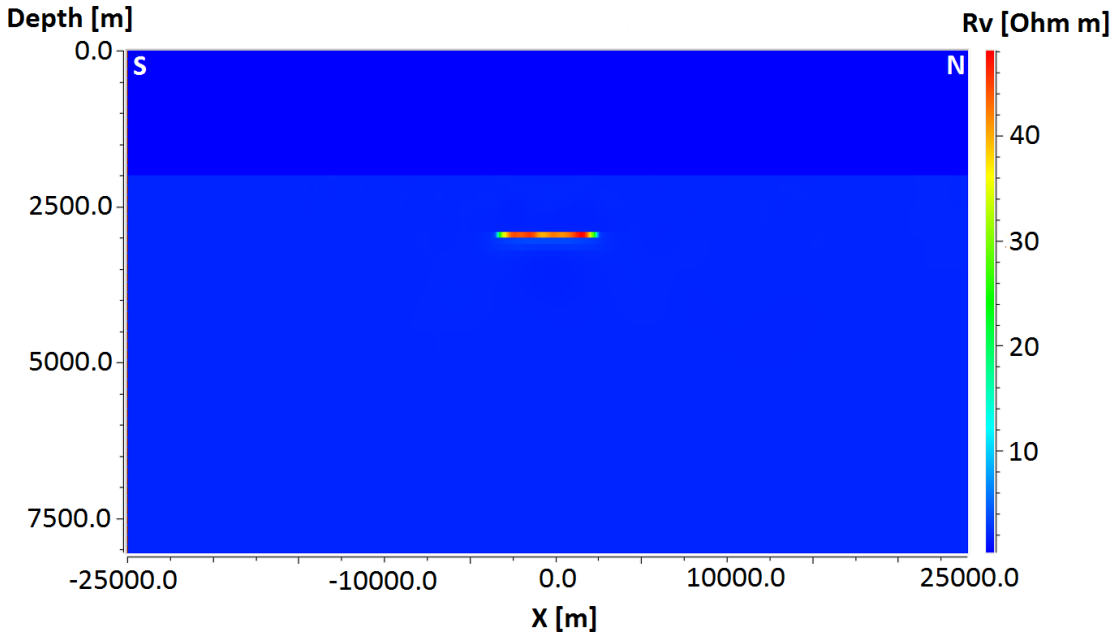

Figure 13: The inversion result for the reservoir at 1000 m burial depth. The seabed is at 2000 m. The reservoir is mapped well, with its true length, thickness and resistivity.

In Figure 14 the reservoir is buried to 2000 m. The reservoir is still imaged clearly, however, it is not mapped as sharply as in the 1000 m burial depth scenario. The maximum resistivity that has been mapped in this case is about 35 Ωm and is lower than for the previous burial scenario. The imaged reservoir has been measured to have a length of 5.6 km, under sizing the imaged reservoir with 400 m. The thickness of the imaged reservoir has increased by 100 m, to a total of about 200 m. The imaged reservoir is also measured to be pulled up by 200 m. In this case the transverse resistance is measured to be approximately 4600 Ωm. The total misfit of the inversion after 99 iterations is 1.026.

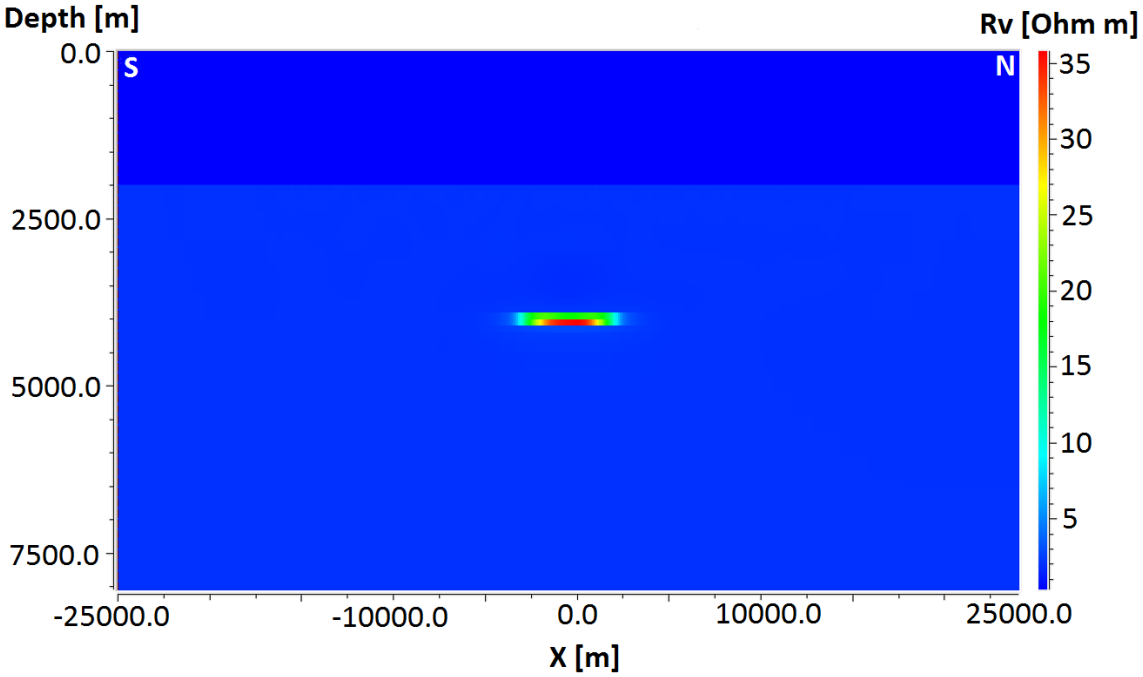

Figure 14: The inversion result for the reservoir at 2000 m burial depth. The seabed is at 2000 m. The reservoir is imaged with lower length and resistivity, and increasing thickness than the true reservoir.

Figure 15 shows the case for when the reservoir is buried to 2500 m. For this case the maximum resistivity mapped is one tenth of the true reservoir resistivity, with maximum resistivity being measured at 10 Ωm. The mapped reservoir becomes more diffuse than for the previously cases, and only the upper boundary of the reservoir is mapped sharply. The imaged reservoir has in Figure 15 been measured to have a length of 5 km, making the imaged reservoir 1 km shorter than its true length. The thickness is measured to be 400 m, which means that it is mapped to be four times the true reservoir. The mapped reservoir is measured to have been pulled up by 250 m from its true burial depth of 2500 m. The transverse resistance for this case is found to be 3100 Ωm. For this case the total misfit of the inversion after 99 iterations is 1.046.

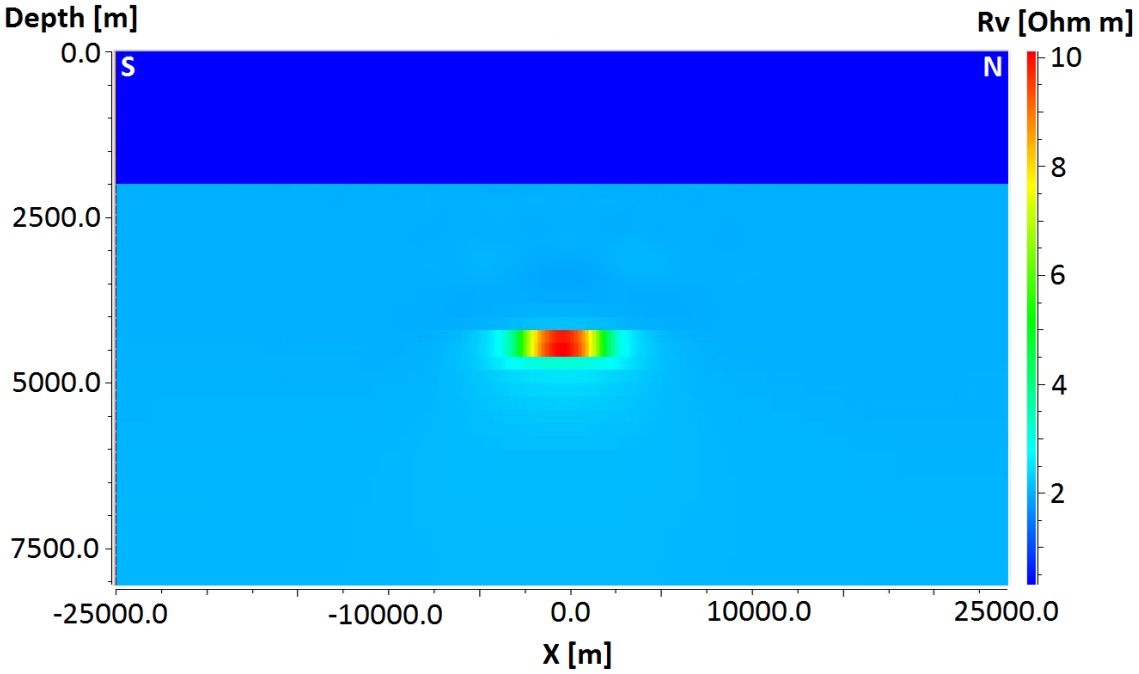

Figure 15: The inversion result for the reservoir at 2500 m burial depth. The seabed is at 2500 m. The reservoir is imaged with significantly smaller length and lower resistivity than the true reservoir. The image is also more smeared out.

In Figure 16 the reservoir is buried to a depth of 3000 m. The mapped reservoir has no sharp edges, and have a oval shape. The imaged reservoir has a resistivity of about 3.5 Ωm, which is only 1.5 Ωm difference from the background resistivity. If the background had not been a homogeneous halfspace, it is doubtful if the inversion would have been able to map the reservoir. However, for this simple case, the inversion manages to map the reservoir well enough for further interpretations. The imaged reservoir is in Figure 16 measured to have a length of 3.6 km. This implies that the imaged reservoir is shortened by 2.4 km compared to its true length. The thickness of the mapped reservoir is measured to be 1 km, which is 10 times the thickness of the true reservoir. For this case the imaged reservoir has been measured to be pulled up 700 m from its true burial depth. The transverse resistance for this case is 1500 Ωm. Given the fact that the transverse resistance has been significantly reduced from the reservoir's true transverse resistance of

5000 Ωm, it is debatable if the result from the inversion is interoperable. The total misfit for the inversion is 1.02 after 78 iterations.

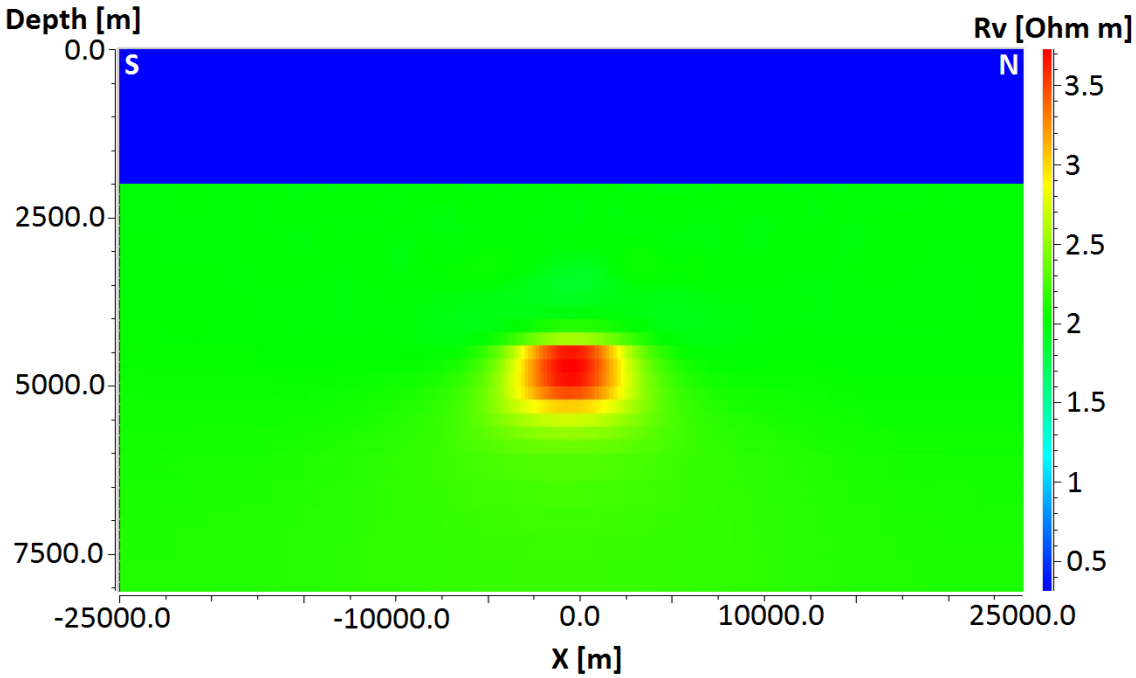

Figure 16: The inversion result for the reservoir at 3000 m burial depth. The seabed is at 2000 m. The reservoir is imaged poorly with low resistivity, and the areal extent is smeared out.

Figure 17 shows the case where the reservoir is buried at 4000 m. In this scenario the inversion has not managed to map the reservoir. The figure shows the halfspace with a resistivity of 2 Ωm, and the water layer with a resistivity of 0.31 Ωm. The total misfit of the inversion is at 1 after a total of 2 iterations.

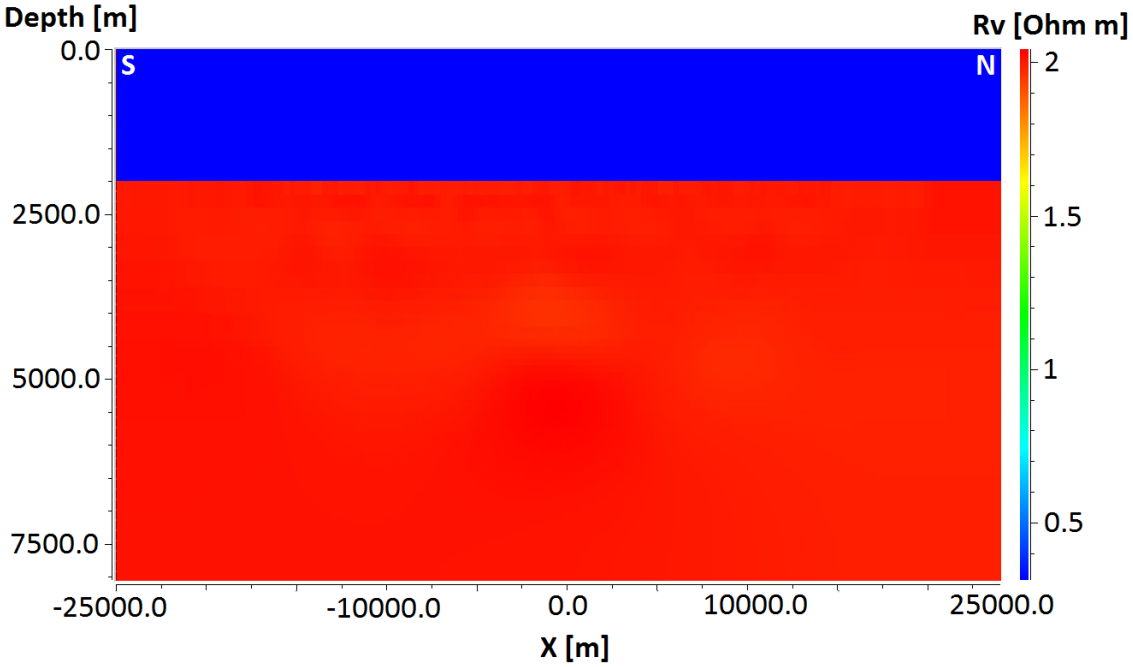

Figure 17: The inversion result for the reservoir at 4000 m burial depth. The seabed is at 2000 m. For this case the inversion has not managed to imaged the reservoir.

From Figures 13 to 17 it is seen that the reservoir becomes imaged with less precision, as the burial depth increases. The reason for this is that the frequencies get attenuated as they propagate deeper into the subsurface, as explained in section 3.2. The pull up effect may be caused by the regularization term in equation 29. The misfit function will choose the model with the lowest misfit, however, the regularization will get a higher value from a model where the reservoir is buried deeper and with a higher resistivity. For this reason the misfit function will choose the model with the shallower reservoir and lower resistivity.

A summary of the inversion result can be seen in table 1.

Table 1: Summary of the inversion results. Increasing burial depth results in decreasing resistivity and length, and increasing thickness.

Reservoir's Burial Depth (m)	Reservoir Length (m)	Reservoir Thickness (m)	Pull Up (m)	Maximum Resistivity (Ωm)	Transverse Resistivity (Ωm)
1000	6000	100	100	50	4300
2000	5600	200	200	35	4600
2500	5000	400	250	10	3100
3000	3600	1000	700	3.5	1500

4.4.2 Comparing the Results of the Mean Square Error and the Inversion

The significance level of 5κ needed to be calibrated to the results from the total mean squared error and the Gauss Newton inversion. This was done by studying Figure 7 for the depths 1000 m, 2000 m, 2500 m and 3000 m, and comparing it to the inversion result. For each of the four depths the first data point above the significant value was located, and the length of the observed reservoir was noted. This is shown in Figure 18, where the four depths have been extracted from Figure 7. As it is observed that the reservoir will always be undersized to some degree during mapping, only the cases where the observed reservoir has been decreased from 6 km to 3.6 km are shown in Figure 18. The black circles in Figure 18 show the first data point above the statistical level limit of 5κ.

From Figure 18 the length of the reservoir can be found for each case where the different burial depths have reached the first point above the significance level. For the burial depth of 1000 m, the reservoir length is approximately 5900 m when the mean squared error is above the significance level. Given that the electromagnetic field is very sensitive to resistivity changes at this shallow burial depth, the mean squared error is 1.12 when the observed reservoir has a length of 5900 m. This mean squared error is higher than then significant value, thus, making it a fair assumption that the length of

the reservoir can be mapped to the true length of 6000 m, for the burial depth of 1000 m.

The burial depth of 2000 m, encounters the first data point above the significance level at a length of the reservoir corresponding to 5700 m. The mean squared error for the burial depth of 2000 m is then at 1.031. The first data point above the significant level for the burial depth of 2500 m is 1.026, where the reservoir is at 5200 m. To reach the first data point above the significant level for the burial depth 3000 m, additional forward modeling was run until the length of the reservoir was reduced to 4300 m. At this point the mean squared error had a value of 1.024.

When comparing the reservoir lengths for the mean squared error above the significance level in Figure 18 to the reservoir lengths measured from the Gauss Newton inversion, it is clear that the data show the same trend as illustrated in Figure 19. However, the results does not seem to be compatible, which means that the assumption of 5κ as statistical significance level is not a valid assumption.

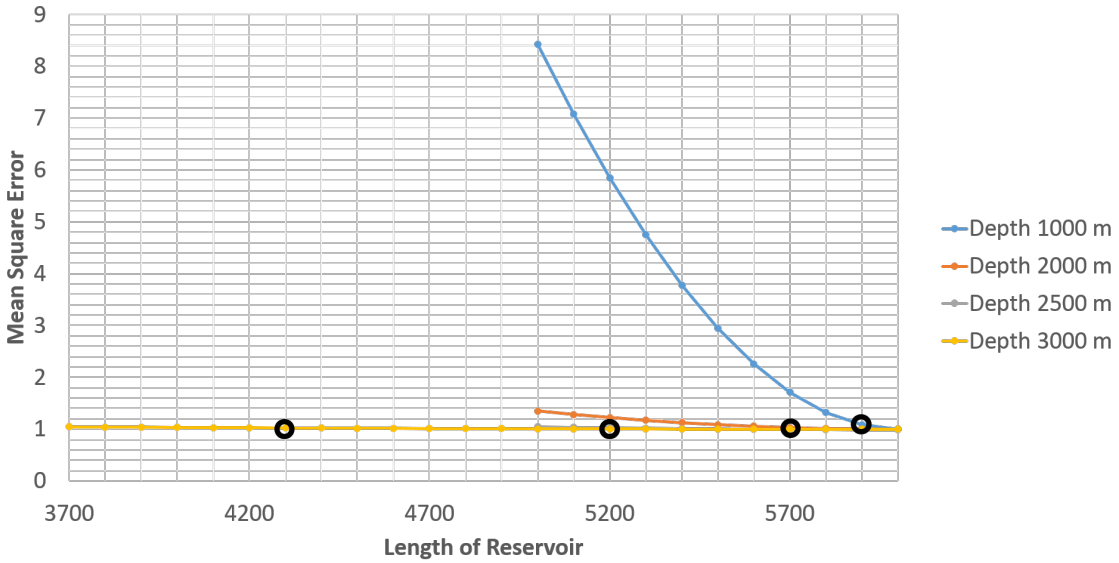

Figure 18: The total mean squared error for the depths 1000 m, 2000 m, 2500 m and 3000 m. The black circles show the first value over the significant value of 1.023154 for each burial depth, assuming 5κ significance level.

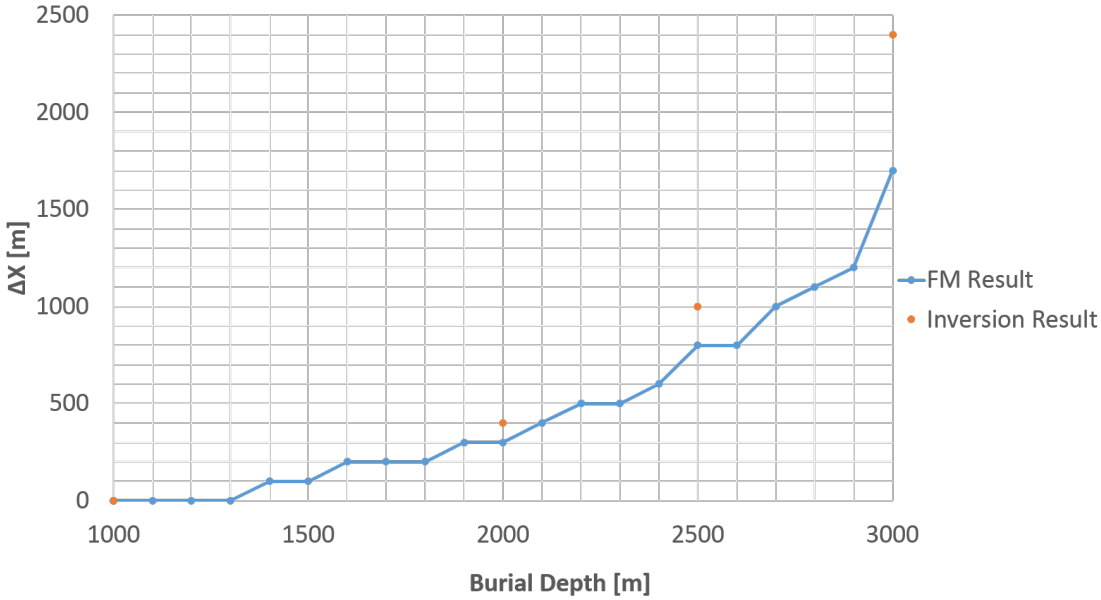

Figure 19: The perturbation in reservoir length vs. burial depth for the mean squared error and inversion result, assuming a significanse level of 5κ. The results from the inversion and forward modeling show the same trend, however, the differences between the inversion result and mean squared error increase with burial depth.

Since the assumption of a statistical significance level of 5κ did not give a good fit between the inversion and the forward modeling result, it is desirable to find a significance level that would give a good fit of the two results. By assuming the statistical significance level is found at 10κ a good fit is found as can be seen in Figure 21. The relationship shown in Figure 21 shows a linear trend up to a burial depth of 2000 m, after which the perturbation seems to increase exponentially with burial depth. With the assumption of 10κ the significance level is at 1.0463, and in Figure 20 the first value above the significance level is circled for the depths; 1000 m, 2000 m, 2500 m and 3000 m.

For the depth 1000 m, the first mean squared value over the significance level gives a reservoir length of 5900 m. However, the mean squared value is at 1.12 which is significant higher than the significance level. Given this, it is

assumed that the length of the reservoir is closer to 6000 m than 5900 m. For the burial depth of 2000 m, the first mean square value above the significance level is 1.0559 and gives a reservoir length of 5600 m, which fits well with the imaged reservoir length measured from inversion. When the reservoir is buried to 2500 m, the first mean squared value above the significance level is 1.0474 and gives a reservoir length of 5000 m, which matches well with the imaged reservoir length. For the burial depth of 3000 m, however, the first mean squared value above the significance level is at 1.0464 which gives a reservoir length of 3700 m. This is reservoir length is 100 m longer than the measured length of the imaged reservoir.

The assumption that the statistical significance level is at 10κ is a very strict assumption. However, it is not surprising one needs a large change in the data for it to result in a change in the imaged model. The assumption of a statistical significance level of 5κ is still a good initial assumption, as the probability is low for changes in the data above significance level. The assumption is however, not valid for changes in the data to correlate with changes in imaged model. This does not mean that the conclusions drawn in section 4.3 is invalid. It can also be seen that the result from section 4.3 is the same using a significance level of 5κ or 10κ, where the statistical significance level of 10κ for each frequency and receiver is 1.498.

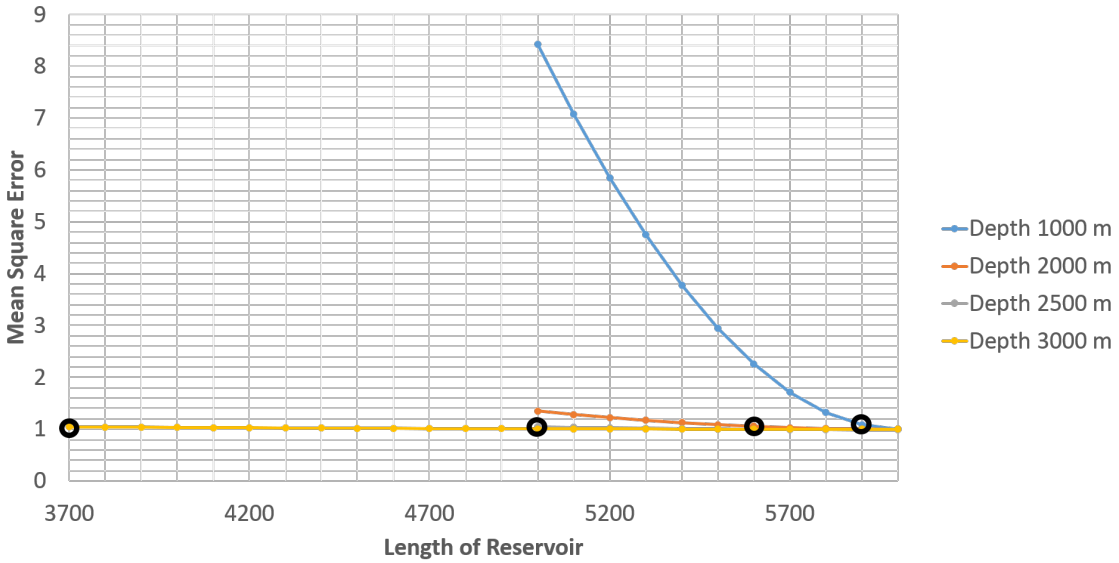

Figure 20: The total mean squared error for the depths 1000 m, 2000 m, 2500 m and 3000 m. The black circles show the first value over the significant value of 1.0463 for each burial depth.

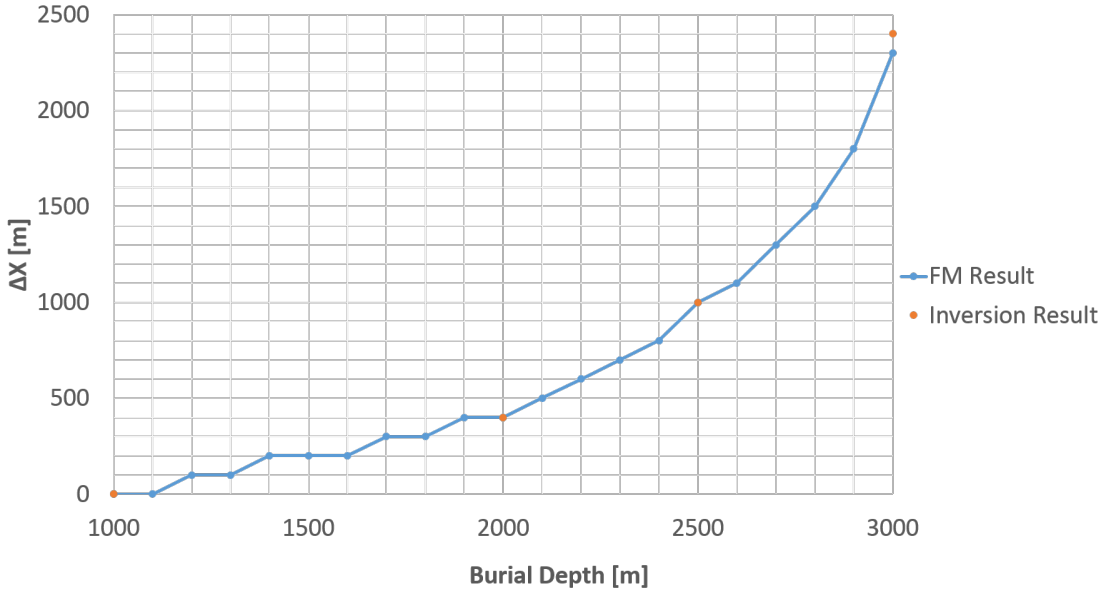

Figure 21: The perturbation in reservoir length vs. burial depth for the mean squared error and inversion result, given a significance level of 10κ. The results from the inversion and forward modeling fit well with each other and show the same trend. Only the last value for burial depth 3000 m have a difference in pertubation.

In Figure 16 the inversion seems to barely be able to map the reservoir at the burial depth of 3000 m, and in Figure 12 all the frequencies are seen to fluctuate around 1, which suggests that the receivers are not able to measure the reservoir at this depth. To investigate if the inversion nevertheless is able to map the reservoir at this depth, or if the imaging in Figure 16 is a result of the noise in the data, the root mean square error (RMS) of the inversion was studied. The plot of the RMS error in the inversion for each iteration can be seen in Figure 22. That data error is the error in the data, and the total error is the error from the data and the regularization term. Given that Figure 22 shows the RMS error, the values need to be squared before they can be compared to the significance level of 1.0463. The initial mean squared error from the data and total error is above 1.21, which is higher than the significance level. At iteration 1 the mean squared error for the data is below 1.036, however, the total significant error has a value of about

1.061. The total significant error does not get below the significant level until iteration 5. This means that the inversion is based on significant data. As a comparison, Figure 23 shows the RMS error in the data for the burial depth 4000 m. It is seen that the mean squared error is below the significant value from the start, hence, explaining why the reservoir has not been mapped as illustrated in Figure 17. Consequently the inversion result from burial depth 3000 m is a significant result.

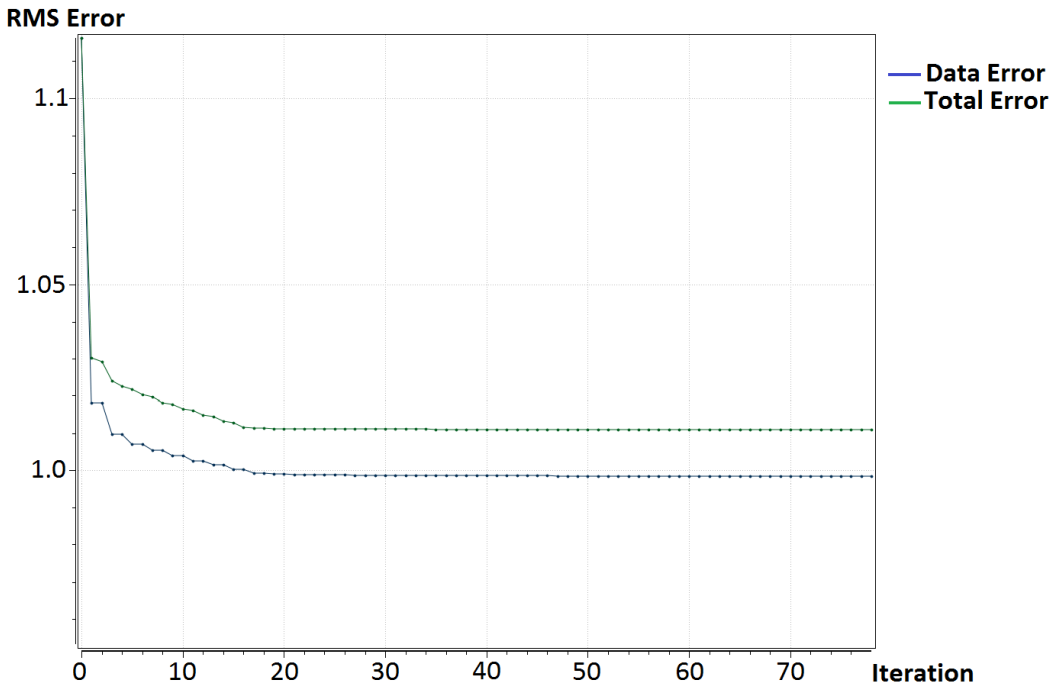

Figure 22: The RMS errors in the inversion for each iteration of the burial depth 3000 m are shown. The data error is the error in the data, and the total error is the sum of the error in the data and the regularization term. The total mean squared error is above the significance level for the first 5 iterations, making the inversion result valid.

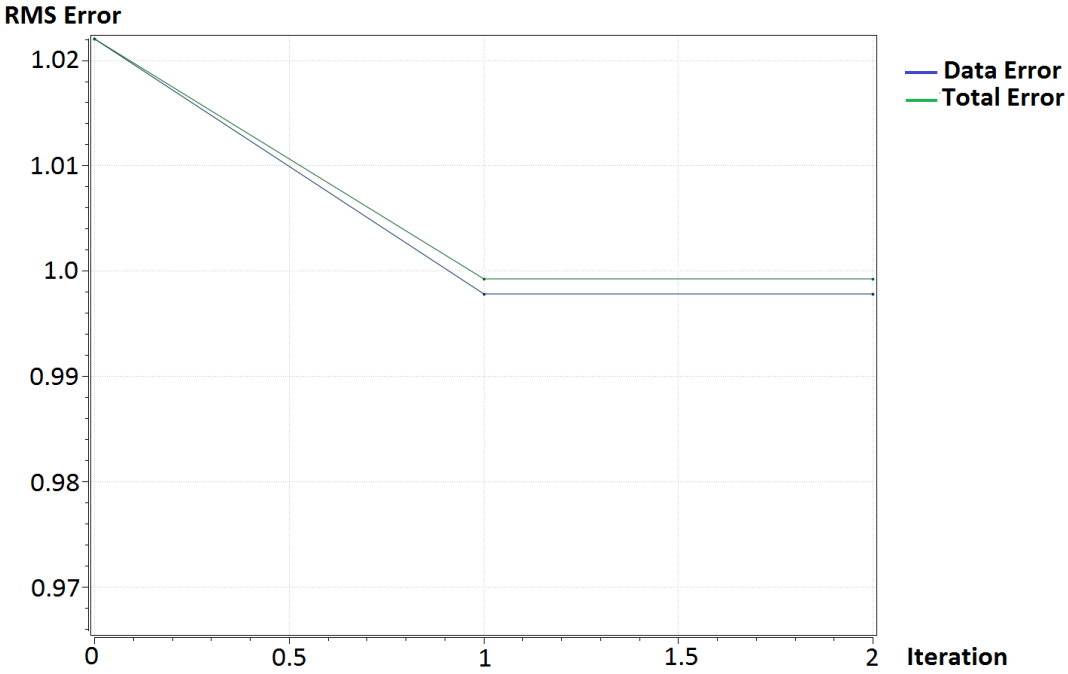

Figure 23: The RMS errors in the inversion for each iteration of the burial depth 4000 m are shown. The data error is the error in the data, and the total error is the sum of the error in the data and the regularization term. The initial mean squared error is below the significance level, making the inversion result invalid.

4.5 Closing Remarks

In summary, it has been demonstrated that by using a statistical level of 10κ the changes in the data and will give a similar change in the imaging of the reservoir. This is illustrated in Figure 21, where the results from the forward modeling and inversion are plotted as perturbation in reservoir length versus burial depth of the reservoir. By using the assumption of 10κ as significance level, the marine CSEM is able to detect a reservoir buried at a depth of 3000 m. Plots of this type, for different scenarios will be beneficial for geophysicists to consult with when doing inversion, as it may help understand how the reservoir will be imaged at different depths.

When reading the results in Figure 21 it is important to keep in mind that it is based on a simple model which may not image a real reservoir correctly. As previously mentioned a reservoir buried at 3000 m depth will be very difficult to map by marine CSEM if there are natural variation in the subsurface. The error will increase with increasing burial depth, making the results in Figure 21 more dependable for the shallower depths.

5 Conclusion

In this study an simple 2D model was investigated where the length and burial depth of the reservoir was varied. By using forward modeling to find the mean squared error, an estimate of the under sizing of a reservoir's length for different burial depth was found. It was found that by using a statistical significance level of 10κ the change in the reservoir length correlated with the change in the image imaged reservoir length.

The perturbation seems to have a linear relationship up to a burial depth of 2000 m, after that the perturbation seems to increase exponentially.

6 Further Work

It is suggested for further work on this topic to use a more complex and, thus, realistic model to see if compatible results are obtained. By using different models to simulate different scenarios, more estimates of the error of the under sizing will be provided. These estimates of the error may be useful for geophysicists to help correct for the under sizing of the reservoirs length. It would also be interesting to make an estimate of the error in the modeled reservoir thickness, and it relation to burial depth, for different scenarios.

References

Ansari, A., A. B. Shaftie, and A. B. M. Said, 2012: Relationship of resistivity contrast and thickness depth of hydrocarbon for seabed logging application. *International Journal of Computer Science Issues*, **9**(3), 214–221.

Archie, G. E., 1942: The electrical resistivity log as an aid in determining some reservoir characteristics. *Petroleum Technology* 54–62.

Becken, M. and R. Streich, 2010: 1D sensitivity of land-based CSEM to thin resistive layers. SEG, Denver, 884-888.

Bhuyian, A. H., M. Landrø, and J. S. E, 2012: 3D CSEM modeling and time-lapse sensitivity analysis for co_2 storage. *Geophysics*, **77**(5), 343–355.

Brown, V., M. Hoversten, K. Key, and J. Chen, 2012: Resolution of reservoir scale electrical anisotropy from marine CSEM data. *Geophysics*, **77**(2), 147–158.

Chlamtac, M. and F. Abramovici, 1981: The electromagnetic fields of a horizontal dipole over vertical inhomogeneous and anisotropic earth. *Geophysics*, **46**(6), 904–915.

Constable, S., 2010: Ten years of marine CSEM for hydrocarbon exploration. *Geophysics*, **75**(5), 67–81.

Constable, S. and C. Weiss, 2006: Mapping thin resistors and hydrocarbons with marine EM methods: Insights from 1D modeling. *Geophysics*, **71**(2), G43–G51.

Cox, C., S. Constable, A. Chave, and S. Webb, 1986: Controlled source electromagnetic sounding of the oceanic lithosphere. *Nature*, **320**, 52–54.

Ellingsrud, S., T. Eidesmo, and S. Johansen, 2002: Remote sensing of hydrocarbon layers by seabed logging (SBL): Results from a cruise offshore angola. *The leading edge* 972–982.

Gao, G., D. Alumbaugh, J. Chen, and K. Eyl, 2007: Resolution and uncertainty for marine CSEM and cross-well EM imaging. SEG, San Antonio, 623-627.

Hansen, K, R. and R. Mittet, 2009: Incorporating seismic horizons in inversion of CSEM data. In *SEG International Exposition and Annual Meeting*, Houston, 633-637.

Johansen, S. E. and P. T. Gabrielsen, 2015: Interpretation of marine CSEM and marine MT data for hydrocarbon prospecting. In *Petroleum geoscience, From sedimentary environments to rock physics*, Bjørlykke, K., editor. Springer, second edition, 515-544.

Kaputerko, A., A. Gribenko, and M. S. Zhdanov, 2007: Sensitivity analysis of marine CSEM surveys. SEG, San Antonio, 609-613.

Keller, G. V., 2006: Rock and mineral properties. In *Electromagnetic Methods in Applied Geophysics.*, Nabighian, M. N., editor. Society of Exploration Geophysicists, 13-51.

Lien, M. and T. Mannseth, 2008: Sensitiviyu study of marine CSEM data for reservoir production monitoring. *Geophysics*, **73**(4), 151–163.

Lu, X. and C. Xia, 2007: Understanding anisotropy in marine CSEM data. In *SEG Technical Program Expanded Abstracts*, San Antonio, 633-637.

Løseth, L. O., 2007: Marine CSEM signal propagation in TIV media. SEG, San Antonio, 638-642.

Maaø, F., 2007: Fast finite-difference time-domain modeling for marine-subsurface electromagnetic problems. *Geophysics*, **72**(2), 19–23.

Mittet, R., 2010: High-order finite-difference simulations of marine CSEM surveys using a correspondence principle for wave and diffusion fields. *Geophysics*, **75**(1), 33–50.

Mittet, R. and J. P. Morten, 2012: Detection and imaging sensitivity of the marine CSEM method. *Geophysics*, **77**(6), 411–425.

Mittet, R. and J. P. Morten, 2013: The marine controlled-source electromagnetic method in shallow water. *Geophysics*, **78**(2), 67–77.

Mittet, R. and T. Schaug-Pettersen, 2008: Shaping optimal transmitter waveforms for marine CSEM surveys. *Geophysics*, **73**(3), 97–104.

Nocedal, J. and S. J. Wright, 2000: *Numerical Optimization*. Society of Exploration Geophysicists, 254, 2 edition.

Norbert, M., 2014: Modeling nad inversion of CSEM data using green's function methods. Master degree in petroleum geoscience, University of Bergen.

Orange, A., K. Key, and S. Constable, 2009: The feasibility of reservoir monitoring using time-laps marine CSEM. 21-29.

Reynolds, J. M., 2011: *An introduction to applied environmental geophysics*. John Wiley & Sons, 289-293, 2 edition.

Streich, R. and M. Becken, 2011: Sensitivity of a controlled-source electromagnetic filds in planarly layerd media. *Geophysics*, **187**, 705–728.

Walpole, R. E., R. H. Myers, S. L. Myers, and K. Ye, 2007a: *Probability and Statistics for Engineers and Scientists*. Pearson Education International, 367-369.

Walpole, R. E., R. H. Myers, S. L. Myers, and K. Ye, 2007b: *Probability and Statistics for Engineers and Scientists*. Pearson Education International, 200-221.

Walpole, R. E., R. H. Myers, S. L. Myers, and K. Ye, 2007c: *Probability and Statistics for Engineers and Scientists*. Pearson Education International, 172-176.

Walpole, R. E., R. H. Myers, S. L. Myers, and K. Ye, 2007d: *Probability and Statistics for Engineers and Scientists*. Pearson Education International, 272-273.

Wang, Z., L. J. Gelius, and F. N. Kong, 2008: A sensitivity analysis of the

sea bed logging technique with respect to reservoir hetrogeneities. SEG, Las Vegas, 711-715.